Journal of Volcanology and Geothermal Research 188 (2009) 277–296

Contents lists available at ScienceDirect

Journal of Volcanology and Geothermal Research

journal homepage: www.elsevier.com/locate/jvolgeores

Seismicity and earthquake hazard analysis of the Teton–Yellowstone region, Wyoming

Bonnie J. Pickering White [a,*], Robert B. Smith [a], Stephan Husen [b], Jamie M. Farrell [a], Ivan Wong [c]

[a] Department of Geology and Geophysics, University of Utah, Salt Lake City, Utah, USA
[b] Swiss Seismological Service, ETH Hoenggerberg, CH8093 Zurich, Switzerland
[c] URS Corp., 1333 Broadway, Oakland, CA, USA

ARTICLE INFO

Article history:
Received 26 May 2008
Accepted 15 August 2009
Available online 29 August 2009

Keywords:
Yellowstone
Teton
fault
earthquake
hazard
seismicity
volcano

ABSTRACT

Earthquakes of the Teton–Yellowstone region represent a high level of seismicity in the Intermountain west (U.S.A.) that is associated with intraplate extension associated with the Yellowstone hotspot including the nearby Teton and Hebgen Lake faults. The seismicity and the occurrence of high slip-rate late Quaternary faults in this region leads to a high level of seismic hazard that was evaluated using new earthquake catalogues determined from three-dimensional (3-D) seismic velocity models, followed by the estimation of the probabilistic seismic hazard incorporating fault slip and background earthquake occurrence rates. The 3-D *P*-wave velocity structure of the Teton region was determined using local earthquake data from the Jackson Lake seismic network that operated from 1986–2002. An earthquake catalog was then developed for 1986–2002 for the Teton region using relocated hypocenters. The resulting data revealed a seismically quiescent Teton fault, at M_L, local magnitude > 3, with diffuse seismicity in the southern Jackson Hole Valley area but notable seismicity eastward into the Gros Ventre Range. Relocated Yellowstone earthquakes determined by the same methods highlight a dominant E–W zone of seismicity that extends from the aftershock area of the 1959 (M_S surface wave magnitude) 7.5 Hebgen Lake, Montana, earthquake along the north side of the 0.64 Ma Yellowstone caldera. Earthquakes are less frequent and shallow beneath the Yellowstone caldera and notably occur along northward trending zones of activity sub-parallel to the post-caldera volcanic vents. Stress-field orientations derived from inversion of focal mechanism data reveal dominant E–W extension across the Teton fault with a NE–SW extension along the northern Teton fault area and southern Yellowstone. The minimum stress axes directions then rotate to E–W extension across the Yellowstone caldera to N–S extension northwest of the caldera and along the Hebgen Lake fault zone. The combination of accurate hypocenters, unified magnitudes, and seismotectonic analysis helped refine the characterization of the background seismicity that was used as input into a probabilistic seismic hazards analysis. Our results reveals the highest seismic hazard is associated with the Teton fault because of its high slip-rate of approximately 1.3 mm/yr compared to the highest rate of 1.4 mm/yr in southern Yellowstone on the Mt. Sheridan fault. This study demonstrates that the Teton–Yellowstone area is among the regions highest seismic hazard in the western U.S.

1. Introduction

The earthquake hazard in the Teton–Yellowstone region is the highest in the U.S. Intermountain region (Petersen et al., 2008). It is not only influenced by lithospheric extension associated with Basin-Range tectonism that extends 700 km west to the Sierra Nevada Mountains, California, but it has the superposition of the effects of Yellowstone volcanic sources that can perturb stresses up to 50 km from the Yellowstone hotspot track, i.e., the effects of the Yellowstone hotspot has a profound effect on seismicity not only on Yellowstone but on the surrounding fault zones of the Intermountain region. These combined fault zones are part of the parabolic-shaped zone of pronounced earthquake activity surrounding the Yellowstone–Snake River Plain volcanic field, encompassing the Teton Range and converges at the Yellowstone Plateau (Smith et al., 1985; Anders and Sleep, 1985; also see the companion paper by Smith et al., 2009-this volume).

To evaluate the earthquake potential and seismic hazard of the Teton–Yellowstone region U.S. (Fig. 1), high-precision earthquake data are needed to understand the seismicity patterns in the area. For the Yellowstone National Park area this type of high-quality data were developed by Husen and Smith (2004) from the Yellowstone seismic network. However similar data have not been available for the Teton area.

In this paper we use earthquake data from the U.S. Bureau of Reclamation's (USBR) Jackson Lake Seismic Network (JLSN) to establish

* Corresponding author. 13451 O'Brien Creek Rd., Missoula, MT 59804, USA. Tel.: +1 406 542 9355.
E-mail address: bonnie_jean19@hotmail.com (B.J.P. White).

0377-0273/$ – see front matter © 2009 Elsevier B.V. All rights reserved.
doi:10.1016/j.jvolgeores.2009.08.015

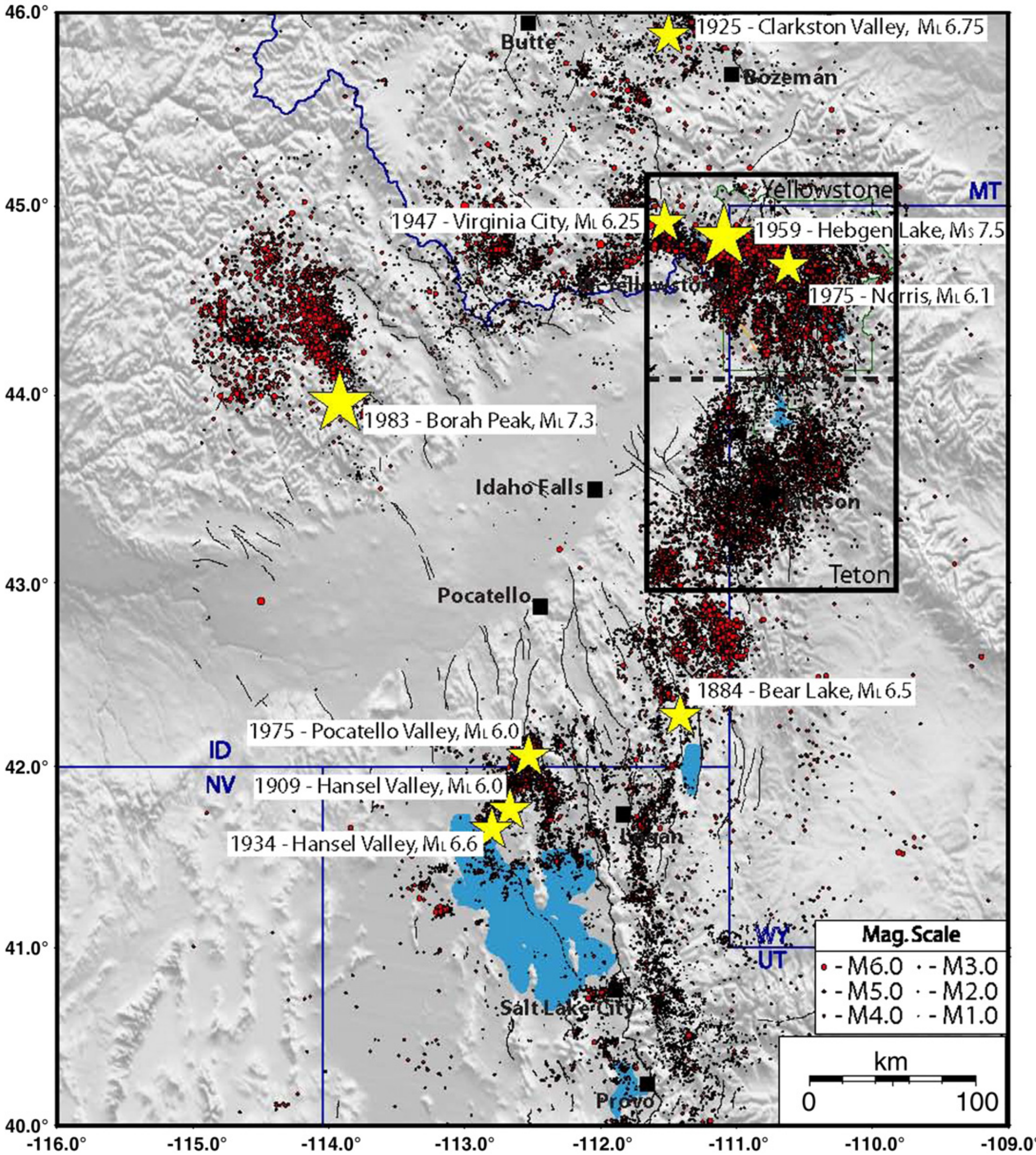

Fig. 1. Epicenter map of the central Intermountain region, Wyoming, Idaho, Montana and Utah showing the Teton and Yellowstone regions are marked by the black box. Earthquake epicenters from ~1850–2005 are shown as red dots and state boundaries are shown by blue lines. Large historic earthquakes and magnitudes are labeled. The earthquake data are from the compilation of historic seismicity of the central Intermountain west by Wong et al. (2000) and updated for earthquake catalog data of the Montana Bureau of Mines and Geology, the Yellowstone seismic network (University of Utah Seismograph Stations, UUSS), the Idaho National Laboratory, the Jackson Lake seismic network, U.S. National Seismic Network and the Utah seismic network (UUSS).

a high-quality earthquake data set for the Teton region, including high-precision hypocenter locations and focal mechanisms. In a second step, this data set was merged with earthquake data of similar quality of the Yellowstone region. The combined data set was then used to derive a preliminary probabilistic seismic hazard assessment for the Teton–Yellowstone region. Our approach includes the relocation of the earthquakes of the Teton region using a probabilistic nonlinear relocation method by incorporating a tomographically determined 3-D *P*-wave velocity (V_P) model that has been derived as part of this study and the computation of focal mechanisms and the stress field for the Teton region. The combination of the earthquake data for the Teton and Yellowstone regions aids in an improved understanding of the seismotectonics of the region, volcanic seismicity and provides a basis for a more accurate seismic hazard evaluation of the region. Our study thus builds upon a preliminary earthquake hazard assessment of the Jackson Lake, Wyoming, dam site by Gilbert et al. (1983) and volcano hazard analysis of Yellowstone (Christiansen et al., 2007).

2. Tectonic setting of the Teton–Yellowstone region

Earthquakes of the Teton–Yellowstone region represent a high level of seismicity of the Intermountain West that is associated with intraplate extension of the Yellowstone hotspot and the surrounding region including the Teton and Hebgen Lake faults. The greater study region is comprised of the Teton Mountain Range, the valley of Jackson Hole, and southern Yellowstone (Fig. 1). This region forms an important part of the Intermountain Seismic Belt (ISB), extending southward 130 km from the Yellowstone volcanic system to the northern Star Valley area of Wyoming and Idaho. For a review on the tectonic–volcanic setting of the Yellowstone region, see the companion paper of Smith et al. (2009) in this issue.

The Teton fault is a youthful normal-fault that bounds the Teton Range in northwestern Wyoming, south of the Yellowstone Plateau volcanic field, and is probably the dominant source of large earthquakes in the Teton area. It is a key feature of the central part of the ISB

(Smith and Sbar, 1974) that extends 1300 km from Arizona through Utah, eastern Idaho, western Wyoming, and western Montana (Fig. 1). The Teton fault is located in the Zone II of the ISB parabolic region of active late Quaternary faults that surrounds the less active region nearest the Snake River Plain (SRP) that are more effected by the thermal effects and flexure associated with the track of the Yellowstone hotspot (Anders et al., 1989; Smith and Braile, 1993). The systematic pattern of late Quaternary faulting paralleling the YSRP differentiated areas of similar-aged faulting and seismicity that we hereby designate as Zones II and III after Smith and Braile (1993). The fault zones are identified on the basis of recency of slip, not on fault direction, and are generally in the directions of oblique- to orthogonal, where the zones encompassing the faults of common age are generally parallel the boundaries of the SRP (Smith and Braile, 1993). Zone II extends outward up to ~40 km from the boundaries of the SRP and is characterized by faults whose most recent displacements are generally older than post-glacial, i.e., generally greater than ~14,000 yr to late Cenozoic age. Zone II was suggested by Smith et al. (1985) as possibly related to a flexural shoulder of the Yellowstone hotspot, while Zone III encompasses the active earthquake zones surrounding the SRP and appears to have been much more active throughout Holocene and historic time than those in Zone II. The active earthquake zone surrounding the Snake River Plain appears to have been most active throughout the late Quaternary and is also interpreted to have been related to the outer edge of the flexural shoulder of the Yellowstone hotspot track based on recency of faulting and height of the associated range front (Smith et al., 1985; Anders et al., 1989). These zones have a similar pattern to the four fault belts defined by Pierce and Morgan (1992) and reproduced in Love et al. (2007).

Regarding the Teton fault, its age of initiation of displacement is problematical. Estimates range from 13 Ma to 2 Ma, based on angular unconformities between the Miocene Colter and Teewinot Formations and the Conant Creek Tuff 3 km east of the Teton Range front (Barnosky, 1984; Love et al., 1992; Smith et al., 1993). The lower tuff on Signal Mountain is now identified as the 4.45 Ma Kilgore Tuff, and the Teton Range was not a significant barrier 5 Ma to flow from the Heise volcanic field when it was deposited (Morgan and McIntosh, 2005). Love (1977) proposed that fault movement began at 5 Ma based on the lack of coarse clastic detritus in lacustrine deposits of Teewinot Formation, 3 km east of the Teton Range front. However, Quaternary to recent deposition of dominantly silt-size and clay-size sediment adjacent to the mountain front and Teton fault in Jackson Lake (Shuey et al., 1977) tends to discount Love's stratigraphically based arguments. Pierce and Morgan (1992) bracketed the activity of the fault after 5 Ma with no tilting offset between 5 and 10 Ma, whereas Leopold et al. (2007) estimated that a large component of Teton Range uplift occurred near ~2 Ma.

The Teton fault has an estimated 10 km of total offset and a long history of post-glacial large, scarp-forming earthquakes. The late Quaternary record of the Teton fault is primarily from fault offsets in moraine and post glacial deposits, in the last 14,000 yr (date based on measurements by Licciardi and Pierce, 2008) These data suggests the occurrence of multiple large scarp-forming earthquakes with moment (M_w, moment magnitude) > 6.5 along its 55 km length (Smith et al., 1993; Byrd, 1994; Byrd et al., 1994).

The Teton fault is divided into three segments with the southern and middle segments extending 42 km from the town of Wilson, Wyoming, north to the south end of Jackson Lake, and the northern segment branches into two segments near the north end of Jackson Lake (Byrd et al., 1994). The paleoearthquake data reveal up to 35 m of scarp height corresponding to a 22 to 28 m fault surface offset, i.e., corrected for hanging-wall back-tilt by Byrd et al. (1994) of post-glacial deposits, i.e., less than ~14,000 yr ago, at String Lake and Trapper Lake areas of the Teton fault (Smith et al., 1993). This corresponds to an average late Quaternary slip rate of about 1.3 mm/yr for the entire fault segment that is among the highest in the Intermountain region of the western U.S. (Byrd et al., 1994). On the basis of its length, the Teton fault is considered capable of generating a maximum earthquake of Mw 7.5 (Wong et al., 2000).

The historic seismicity record reveals however that the Teton fault has been seismically quiescent and occupies a notable seismic gap in the ISB at the $M_L > 3$ level (Smith, 1988). This raises the question if the contemporary stress loading of the fault can be affected by the unusually high deformation rates of the nearby Yellowstone caldera, 15 km to the north (Hampel et al., 2007). Like many other late Quaternary normal faults of the ISB such as the Wasatch, UT, Madison, Mission, Lemhi, and Centennial faults in Montana contemporary seismic quiescence seems to be a common characteristic of these faults with long return times for small-to-moderate magnitude events. Notably the Thousand Springs segment of the Lost River fault was quiescent before the 1983 Borah Peak, ID, earthquake (King et al., 1987). Perhaps long periods of seismic quiescence are typical behavior for normal faults in the ISB.

3. Teton earthquake data

The USBR recorded earthquakes in the Teton region from 1986 to 2002 by a 20-station seismic network focused on the Jackson Lake dam termed the Jackson Lake Seismic Network, JLSN (Fig. 2). Data from the network included seismic waveforms, first arrival *P*-wave picks, and a catalog of earthquake locations that were determined using a 1-D velocity model. Initially, the JLSN consisted of 16 short-period (1 Hz) vertical-component seismograph stations. An additional four stations were installed in 1990 to improve monitoring coverage.

More than 8000 earthquakes, M_L 0.1 to 4.7 were recorded by the JLSN during the reporting period. The largest event reported in the period was a M_L 4.7 earthquake that occurred on December 28, 1993 in the Gros Ventre Range, east of the Jackson Hole Valley and 20 km east of the Teton fault.

Earthquake data from the network was automatically processed in real time, and phase arrivals for local earthquakes, $M_L \geq 2$, along with selected smaller events were manually analyzed and reprocessed by a seismologist. Routine processing of these data included estimations of magnitude, hypocenters determined from a 1-D velocity model, focal mechanisms, and seismic moments.

For the *P*-wave arrival times, the phase timing errors ranged from ± 0.03 to ± 0.3 s with an average error of ± 0.15 s. The average RMS (root-mean-square) residual value for the 8537 hypocenters determined from a 1-D velocity model was 0.12 s that was derived from a total of 95,091 *P*-wave picks and 37,177 S-wave picks. These data were then employed in a new 3-D analysis of seismic velocities, followed by precisely relocating the earthquakes of the Teton area.

3.1. Three-dimensional P-wave velocity model

We used the concept of the "minimum 1-D seismic velocity" model (Kissling, 1988; Kissling et al., 1994) to compute a starting model for the Teton region. This model was also used to select a subset of high-quality events for the 3-D inversion. To jointly solve for hypocenter locations and the 3-D velocity field in this nonlinear problem, we employed the computer code SIMULPS14 (Thurber, 1983; Eberhart-Phillips, 1990). This program was extended by Haslinger and Kissling (2001) for full 3-D ray shooting. The complete explanation of the methodology for solving the coupled hypocenter-velocity problem in the SIMULPS14 program is given by Eberhart-Phillips (1990) and Thurber (1983).

The Teton earthquake catalog consisted of data from 8537 earthquakes that were relocated using the minimum 1-D velocity model and the probabilistic relocation method NonLinLoc (Lomax et al., 2000). Hypocenter locations that had the smallest errors, as given by the a posteriori probability density function (PDF), were chosen to be

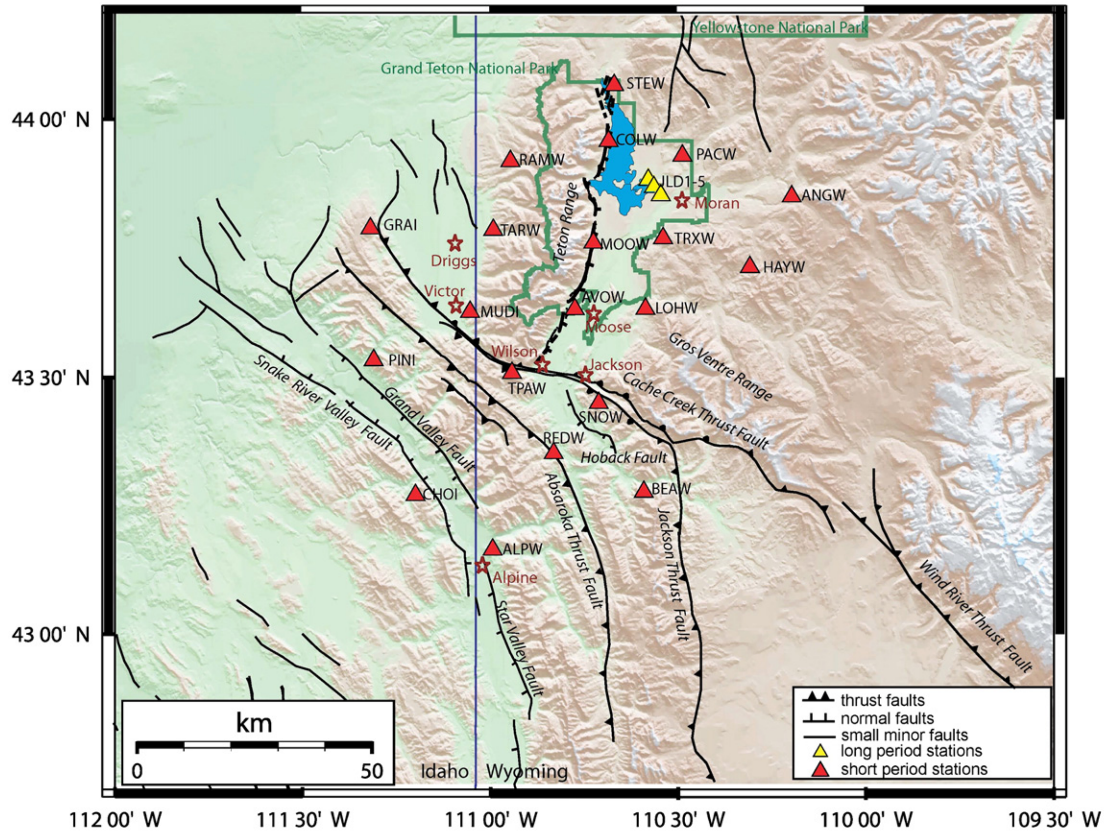

Fig. 2. Seismic stations of the Jackson Lake Seismic Network (JLSN), 1986–2002, used in this study (shown by red and yellow triangles). The Teton fault and other faults in the area are shown by the black lines with their descriptions in the legend. Towns are shown by brown stars.

used in the 3-D velocity model inversion. All selected events had uncertainties that were ellipsoidal in shape. On average the horizontal errors were less than 1 km as determined from the length of the half axes of the corresponding 68% confidence ellipsoids; errors in depth were much larger by 2 or 10 times that of the horizontal errors. Therefore, hypocenter locations fitting the prior selection criteria with a vertical error less than 5 km were selected to be used for the 3-D velocity inversion. The vertical error limit was selected so the highest quality hypocenters would not have a depth error greater than the depth spacing in the 3-D velocity model grid e.g., 5 km. In total, 2056 events with 30,904 *P*-observations were selected to be used in the 3-D *P*-velocity (V_P) inversion.

Parameterization of the 3-D V_P model was based on average station spacing and earthquake distribution throughout the Teton region. We choose our model parameterization by running single-iteration inversions for different model parameterizations ranging from 15 × 15 km to 5 × 5 km. The final grid spacing of 10 × 10 km for the entire Teton region represents the finest possible model parameterization without showing strong heterogeneous ray coverage. Depth spacing varies from 5 km in the upper layers to 10 km in the lowest layers. A finer model parameterization of 5 × 5 km was chosen for the central part of the model where station and earthquake distribution was densest. We first inverted for the coarse model followed by an inversion for the finer model. This gradual approach yields a smooth and consistent velocity model for the entire Teton region with a higher resolving part in the center of the model.

We used resolution estimates such as the diagonal element of the resolution matrix (RDE) and tests with synthetic velocity models, such as checkerboard and characteristic model tests (Husen et al., 2004), to assess the solution quality for the final 3-D Vp model. Checkerboard and characteristic model test results displayed a good solution quality in the center of the seismic network at 0, 5, and 10 km depth. At these depths, single node anomalies are showing almost 95% amplitude recovery.

The resulting seismic tomographic images for the final Teton area are shown in Fig. 3 at the surface, i.e. 0 km depth, which is equal to sea level and corresponds to the average depth of the sediment basins in the Teton region. The three main sediment basins are marked A, B, and C. Basin A reflects the Jackson Hole Valley from northern Jackson Lake to the town of Jackson. Basin B represents the Teton River Valley on the west side of the Teton Range and basin C represents the Grand/Star Valley, Idaho, between the Grand Valley fault and Star Valley fault on the Wyoming–Idaho border. At 5 km depth, low-velocity zones are present in the Jackson Hole Valley, but are more localized beneath the Jackson Lake Dam site, and in an area south of Jackson.

Two distinct patterns are seen in the low velocity zones in the region. Notably, there is a trend of low-velocity upper crustal rock from the Jackson Lake Dam southward to the vicinity of Jackson and an area further south near the southern end of the Palisades Reservoir area (Fig. 3). A detailed discussion of the Teton region tomography by White (2006) suggests that these are separate low-velocity zones but their connection is not resolvable given the resolution capability of our data and model parameterization.

The second notable trend of the low velocity zones extends from the southeast beneath the Jackson Hole Valley towards the town of Jackson, WY. This elongated anomaly trends about a 45-degree angle to the northeastward trend of the southern Teton fault and notably correlates with the much older, Laramide-aged Cache Creek thrust fault zone that extends along a similar southerly trend as the Teton fault. The Cache Creek thrust sheet is part of the larger Laramide foreland family of basement-involved structures like the nearby Gros Ventre and the Wind River Range. The southeast Idaho lineament is

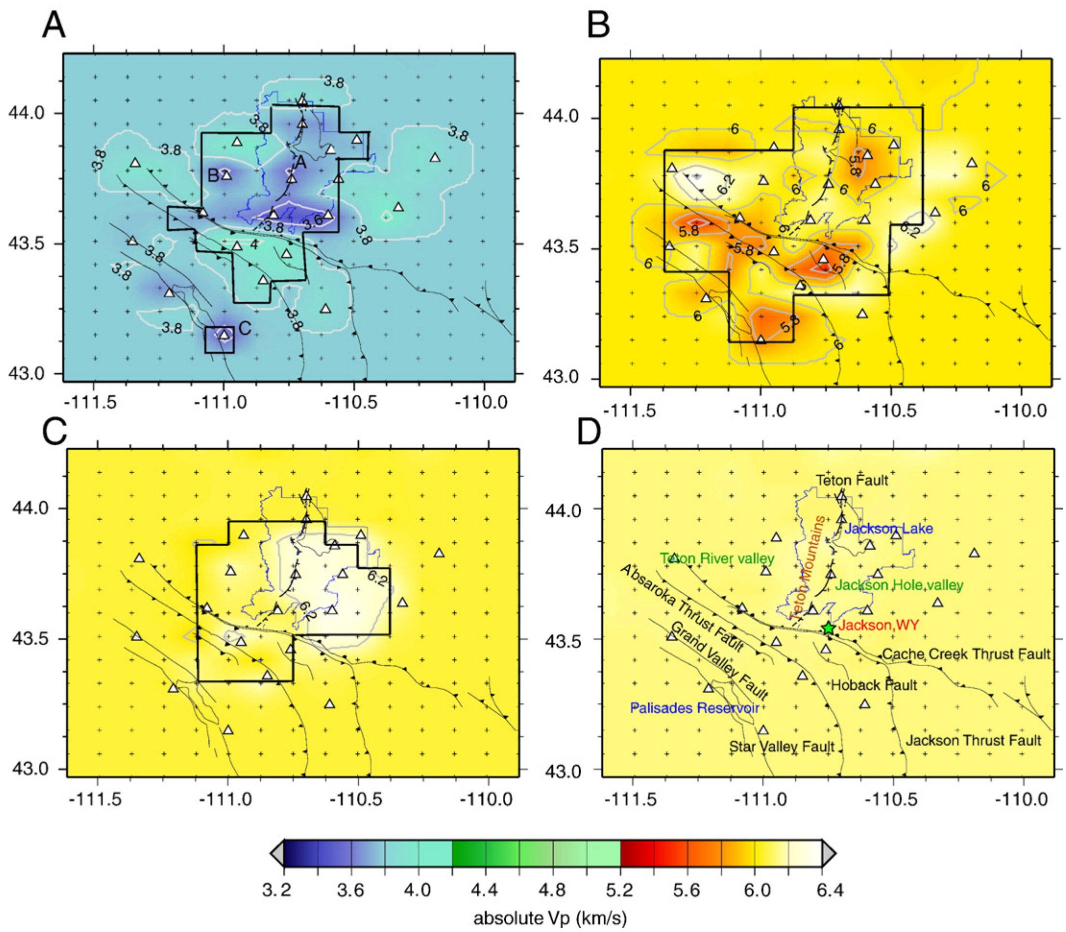

Fig. 3. Horizontal plan view of the final three-dimensional velocity models with absolute velocity values and contours. Seismic stations are marked by the white triangles. Figure (A) displays the velocity contours at 0 km (mean sea level) and area A represents the Jackson Hole Valley basin, area B represents the Teton River Valley basin, and area C represents the Grand Valley basin; (B) displays the velocity contours at 5 km depth, and figures (C) and (D) display velocity contours at 10 km and 15 km depth. Major faults and basin names are shown in (D). Velocity contours are in intervals of 0.2 km/s. Inside the bold rectangular polygons represent the areas of good resolution determined by the synthetic tests and row of resolution matrix plots.

geometrically interpreted to be a lateral ramp that spans the Sevier orogenic belt of southeast Idaho and western Wyoming (Lageson, 1992).

Another feature is that the sediment basins are interpreted to be limited to about 2 to 3 km depth. The low velocity zones imaged at 5 km depth in Fig. 3B are interpreted to be reflecting deeper sediment-filled tectonic basins. At 10 km depth, there is a small high-velocity zone beneath the Jackson Hole Valley that extends across the southern half of Jackson Lake and into the Gros Ventre Range. This feature is well resolved and is possibly an indication of higher velocity bedrock located beneath the Jackson Hole Valley block.

Table 1
Quality class definitions for earthquake locations of the Teton earthquake catalog.

Quality class	Selection criteria
A (excellent)	RMS < 0.5 s, DIFF < 1.0 km, average error < 3.0 km
B (good)	RMS < 0.5 s, DIFF < 1.0 km, average error > 3.0 km
C (questionable)	RMS < 0.5 s, DIFF ≥ 1.0 km
D (poor)	RMS ≥ 0.5 s

The uncertainties used to define the classes are: the difference between the maximum likelihood and expected hypocenter locations, the total event RMS value, and the total average error determined by the average length of the three axes of the 68% error ellipsoid. This same methodology was used by Husen and Smith (2004).

3.2. Earthquake hypocenter relocation

The Teton region earthquakes were relocated using the algorithm NonLinLoc (Lomax et al., 2000). The NonLinLoc program has the ability to employ the 3-D V_P model as determined in the previous section for the Teton region in the relocation process. In total, we relocated 8537 events for the period 1986–2002.

The posterior probability density function PDF as computed by NonLinLoc represents a complete, probabilistic solution to the earthquake location problem, including information on uncertainty and resolution (Lomax et al., 2000). The final hypocenter location is given

Table 2
Event types from the high quality relocated hypocenters.

Rake angle	Type of faulting	High quality events
22.5° ≥ rake > −22.5°	Left-lateral strike-slip	131
−22.5° ≥ rake > −67.5°	Oblique–normal left–lateral strike-slip	110
−67.5° ≥ rake > −112.5°	Normal	111
−112.5° ≥ rake > −157.5°	Oblique–normal right–lateral strike-slip	141
−157.5° ≥ rake > 157.5°	Right-lateral strike-slip	121
157.5° ≥ rake > 112.5°	Oblique–reverse right–lateral strike-slip	19
112.5° ≥ rake > 67.5°	Reverse	6
67.5° ≥ rake > 22.5°	Oblique–reverse left–lateral strike-slip	23

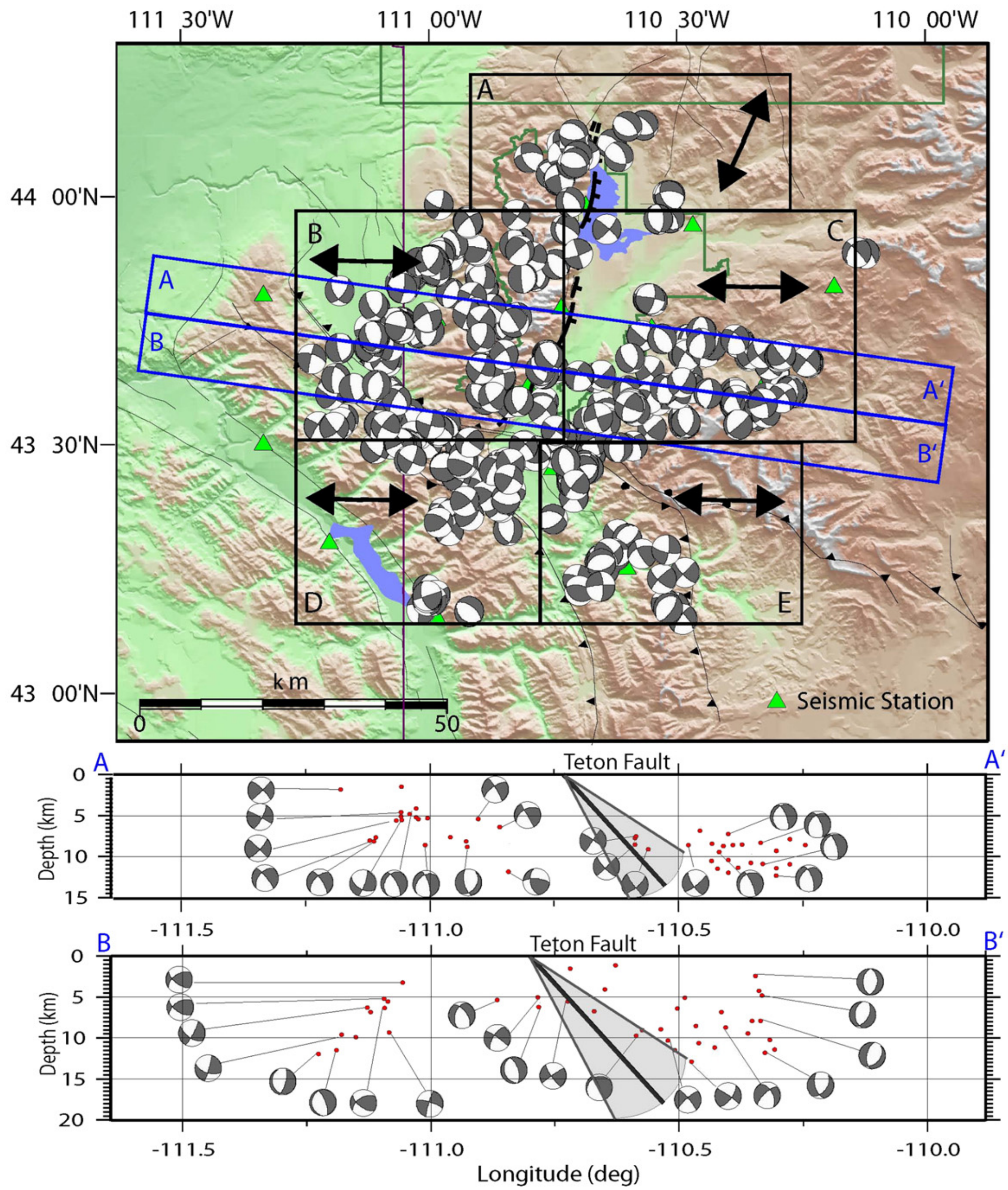

Fig. 4. Focal mechanisms (663) for the Teton region. Seismic stations are shown as green triangles. Note that focal mechanisms that are not within the boxes were not used in the inversions. The thick black arrows indicate the direction of σ_3 and average *T* axes orientations derived from focal mechanisms. The subareas break the Teton fault into five blocks. Block A represents the northern part of the Teton fault and B and C blocks represent the middle footwall and headwall sections. The D and E blocks display the $\sigma 3$ stress orientations in the southern footwall and headwall sections of the Teton fault. Cross sections from A to A′ and B to B′ are shown in blue. Focal mechanisms shown at depth are displayed for selected hypocenters in red with the Teton fault projected at a 45 degree angle.

by the maximum likelihood point of the PDF. In addition to the location uncertainties included in the probabilistic solution, NonLinLoc computes traditional Gaussian estimates such as the expectation hypocenter location and the 68% confidence ellipsoid (Lomax et al., 2000). For well-constrained hypocenter locations, maximum likelihood and expectation hypocenter locations are close and location uncertainties are well represented by the 68% confidence ellipsoid.

We followed the approach of Husen and Smith (2004) to classify the obtained hypocenter locations in four quality classes A, B, C, and D (Table 1). Definition of the quality classes is based on the final RMS, average length of the half axes of the 68% confidence ellipsoid, and the difference between maximum likelihood and expectation hypocenter locations. We chose a difference of 0.5 km between the maximum likelihood and expectation hypocenter locations to differentiate between ill-conditioned (quality class C) and well-conditioned (quality classes A and B) hypocenter location locations. The choice of 0.5 km was based on the analysis of a large number of scatter plots and all of them indicated, that, in general earthquakes with a difference > 0.5 km had large uncertainties of several kilometers in epicenter and focal depth.

A small number of events (less than 1%) fall into the D quality class showing RMS values greater than 0.5 s (Table 1). Given the large RMS values, these events were not used in interpreting the seismic profile of the Teton region. Events in class C, which make up 56% of the catalog, may have location uncertainties of several kilometers often caused by either a low number of observations or locations outside the Teton seismic network giving them a poor azimuthal distribution of observations.

The last two quality classes A and B (representing 53% of the events) are the most reliable earthquake locations in the relocated catalog. All of these events have a well defined PDF with one local minimum, and the 68% confidence ellipsoid represents the location uncertainties accurately. The epicenters in both classes are well defined with differences less than 1 km between the maximum likelihood and expectation hypocenter locations. The error in depth is larger than 3 km for events in class B, and the depth error is less than 3 km for events in class A (Table 1). This larger depth error in class B is due to the lack of stations within the critical focal depth distance, giving a poor constraint on the true vertical depth. The largest depth error for class B was found to be 5 km.

Overall, the relocated hypocenters in the Teton region are much improved in accuracy using the 3-D V_P model and probabilistic relocation method. Travel-time residuals of the relocated Teton hypocenters were improved by 59% relative to the original USBR's 1-D hypocenter locations. On average, hypocenter locations shifted by 0.15 km in epicenter and 1.6 km in focal depth. Relocated hypocenter locations show tighter clustering in epicenter and in focal depth when compared to the original USBR's 1-D hypocenter locations.

3.3. Focal mechanisms and stress field inversion

First motion *P*-wave focal mechanisms have been determined for the study area using the algorithm MOTSI, developed by Abers and Gephart (2001). This technique uses the first arrivals on the seismogram, determines the nodal planes without regard to a priori stress conditions, and uses a statistical approach using *P*-wave polarity data and take-off angles. This program was also used in calculating the stress field solutions from focal mechanisms. The method assumes that the stress field is homogeneous throughout the inversion volume in both space and time (Waite and Smith, 2004). The program varies the values of strike, dip, and rake over given intervals on a grid, and determines the normalized misfit between the planes and the observed first-motion data at each interval. The fault slip direction is assumed to be parallel to the direction of maximum shear stress, which is a result of the inversion. Thus with this method, the first-motion data are weighted on the basis of the analyzed seismograms permitting a better estimate of the full error in the stress solution (Waite and Smith, 2004).

Earthquakes in the Teton region were of small to moderate magnitude, less than M_L 4.0, requiring that accurate first-motion determinations can often only be made from records from the nearest seismograph stations. Therefore, we restricted focal mechanism determination to only high quality Class A quality events with at least six clear, first-motion picks and required that the nearest station be within an epicentral distance of 1.5 times the focal depth to ensure the most accurate focal depth. The selection criteria reduced the number of earthquakes to 663 with 6294 first motion picks. Station polarity reversal corrections did not have to be made due to the results from comparisons of regional network data with well-recorded teleseisms.

The highest weights in the inversion are given to data that are the farthest from the nodal planes where the theoretical *P*-wave amplitude is largest and the probability of a mispick is lowest. The Teton data set consists of events with an average of 8 first motions that are not generally uniformly distributed.

The majority of the focal mechanisms for the Teton region range revealed normal to oblique strike-slip faulting events, with a few thrust solutions. The dip of the nodal planes in the focal mechanisms closest to the Teton fault projection, revealed an east-dipping plane. The solutions were sorted into faulting types based on strike, dip, and rake orientation following the convention of Aki and Richards (1980) (Table 2). Since these categories are based on fault slip angles, we had to determine which of the two nodal planes was the correct fault plane in order to determine the proper rake. For each focal mechanism, the fault plane was chosen as the nodal plane that most closely matched the orientation of faults in the vicinity as mapped by Love et al. (1992) and Byrd et al. (1994).

To determine the stress model for the Teton region, the focal mechanism data were divided into smaller areas based on regions with similar tension (*T*) axes or σ_3 orientations to distinguish regions of relative homogeneous stress (Fig. 4). Constraining all of the focal mechanisms in the data set into one stress tensor degrades the misfit due to the strong heterogeneity in the data set, but this can be corrected by subdividing the data set into areas of homogeneous stress. Stress model solutions were computed on the five smaller areas and all showed signs of homogeneity with the derived *P* and *T* axes for the final focal mechanism and stress tensor calculations. We compared focal mechanisms that were constrained to have slip in the direction of maximum shear stress with those computed independent of the stress field using two measures to quantify the differences. The *P* and *T* axis plots in Fig. 5 are also used in examining the differences between the stress-constrained and unconstrained mechanisms. It is difficult to track changes in individual mechanisms in these plots, and constraining the mechanisms tends to cluster the *P* and *T* axes (Waite and Smith, 2004).

The pattern of *T* axis rotation from NE–SW in area A near the Yellowstone caldera southward to the predominant E–W trend in the Teton Valley is reflected in the stress-field σ_3 orientations (Fig. 5). The σ_3 orientations in all areas are well constrained and near horizontal everywhere. The stress model for area A is poorly constrained and the 68% confidence region for the σ3 overlaps those of the other areas. However, the good agreement of the best-fit σ_3 with the *T* axes in that area, and stress inversion done in the Yellowstone region for this same area gives us some confidence that the rotation of σ3 is realistic.

4. Earthquake patterns of the Teton–Yellowstone region

The new Teton earthquake data were then merged with the Yellowstone earthquake catalog data of Husen and Smith (2004) to create a uniform earthquake catalog of the Teton–Yellowstone region (Figs. 6 and 7). This new data set contains 36,565 earthquakes recorded between 1986 and 2002. Overall, hypocenter locations in the Teton–Yellowstone region are much improved in accuracy using the 3-D V_P models and probabilistic relocation method than previously available. The new earthquake catalog shows tighter clustering of epicenters and focal depths when compared to original hypocenter locations.

Seismicity in the Yellowstone region has been described in various studies (see for example a summary by Husen and Smith, 2004 or the accompanying overview paper by Smith et al. (2009), in this issue). However our homogenous earthquake data provide a uniform set of high quality hypocenters that is required for tectonic and volcanic structural analyses and related hazard assessments. For the Yellowstone area the most intense seismicity occurs northwest of the Yellowstone caldera between Hebgen Lake and the northern rim of the caldera (Fig. 7) with focal depths between 3 and 10 km. Seismicity correlates with late Quaternary faults associated with the Hebgen Lake fault zone (Smith and Arabasz, 1991; Miller and Smith, 1999). The largest of these faults is the Hebgen Lake fault (Fig. 7), but similar farther east structures must be buried underneath rhyolite flows of the Yellowstone Plateau volcanic field.

The northwestern Yellowstone region is also the locus of several large and intense earthquake swarms, including the largest historic earthquake swarm in Yellowstone in 1985 (Waite and Smith, 2002; Farrell et al., 2009-this volume). New interpretations by Farrell et al. (2009-this volume) suggest that many of these swarms may be associated by migration of hydrothermal and other fluids released by the crystallization of magma beneath the Yellowstone caldera, as postulated for

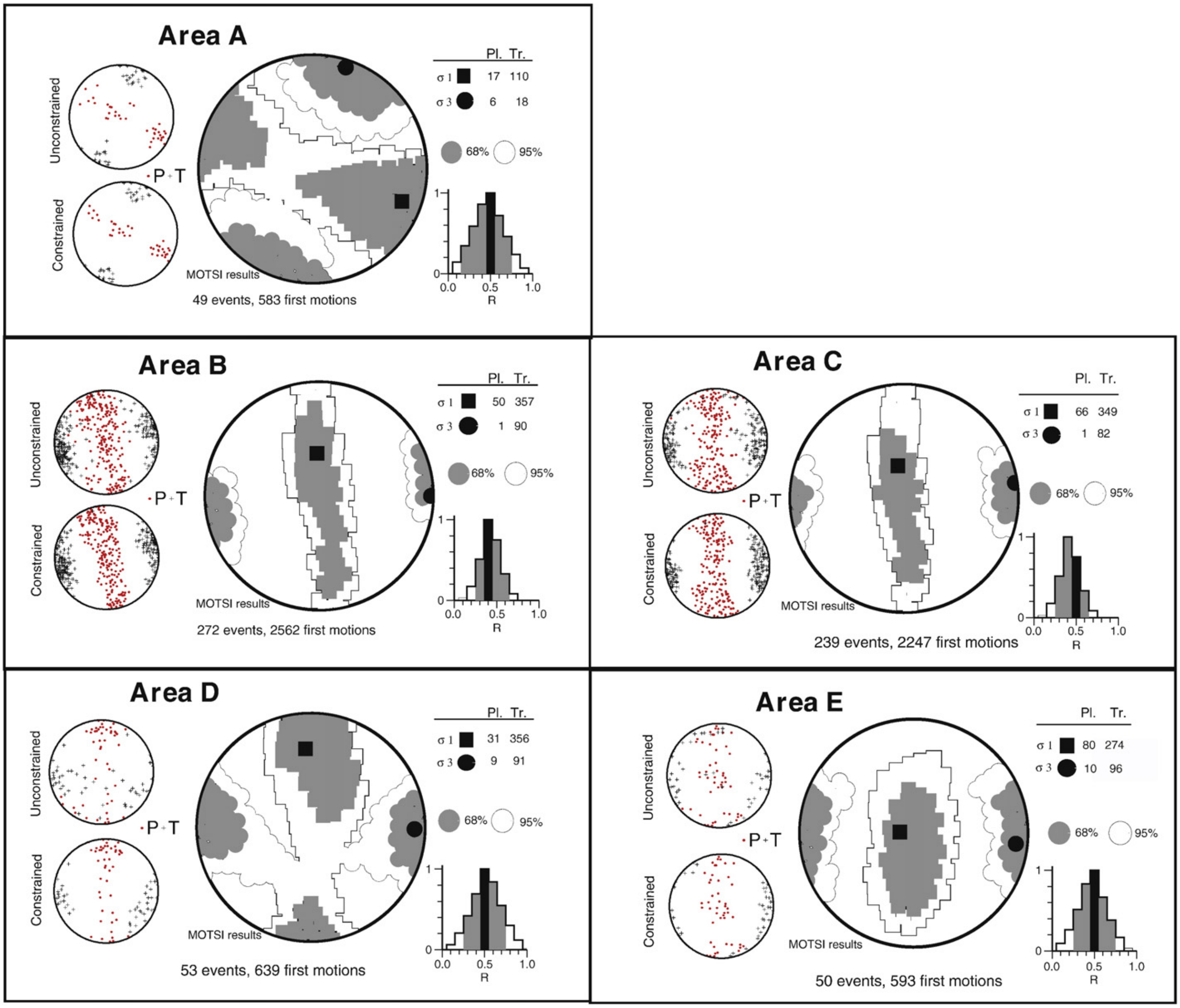

Fig. 5. Stress field solutions computed for the five small areas A–E in the Teton region using MOTSI. The *P* and *T* axes for all earthquakes in each area are shown for focal mechanisms unconstrained and constrained by the stress solution. Best fitting σ1 and σ3 are plotted with black squares and circles. The plunge (Pl.) and trend (Tr.) of each is listed. The 68% confidence regions are shown in gray and the 95% confidence regions are white. Subdivisions were designed to minimize any possible heterogeneities in the stress field of the overall region. Areas were initially chosen based on areas of similar *T* axis orientations.

the 1985 earthquake swarm. Epicenters in the Yellowstone caldera is generally diffuse but some reveal a general north–south orientation. Seismicity here is also characterized by clusters of mainly shallow earthquakes (< 5 km focal depth), sometimes associated with larger hydrothermal areas (Fig. 7). Notable seismicity has been associated with the Norris Geyser Basin area extending to the northern rim but outside of the Yellowstone caldera. This includes a 1975 M_L 6.1 earthquake located 15 km southeast of the caldera boundary that was the largest caldera earthquake in the historic record (Fig. 7). Hypocenter locations show a notable shallowing of earthquakes across the Yellowstone caldera (Waite and Smith, 2002; Smith et al., 2009-this volume), that is explained by shallowing of the brittle-to-ductile transition zone due to elevated temperatures associated with the crustal magma reservoir.

Seismicity between the Yellowstone and Teton regions shows distinct linear N–S trends (Fig. 7) that continue across the southern part of the Yellowstone caldera to the west of the large north–south trending faults such as the Mt. Sheridan fault system and the Buffalo Fork and Yellowstone Lake fault systems. Moreover a N–S band of seismicity extending from the northern end of the Teton fault northward beneath the southern part of the Yellowstone caldera suggests that it reflects pre-existing zones of weakness along earlier faulting associated with Basin-Range extensional processes (Smith and Arabasz, 1991).

In the Teton region, the hypocenter patterns reveal distinct seismic trends that can be seen throughout the area (Fig. 6). We believe that these seismic trends reflect seismogenic features such as buried faults and pre-existing zones of weakness that may be related to older Laramide and Sevier thrust and fold belt faults and fractures. These earthquake clusters are consistent over different time periods and their focal mechanisms show similar faulting types with similar strikes.

Most obvious is the persistent zone of epicenters in the Gros Ventre Range, east of the Jackson Hole Valley, marked by trends 1 and 2 in Fig. 6. These linear trends correlate well with southeast-trending valleys in the Gros Ventre Range. The focal mechanisms of these earthquakes reveal dominantly normal faulting with a small oblique strike-slip component (Fig. 4). Earthquakes in the Gros Ventre Range regularly occurred throughout the recorded time period from 1986 to 2002.

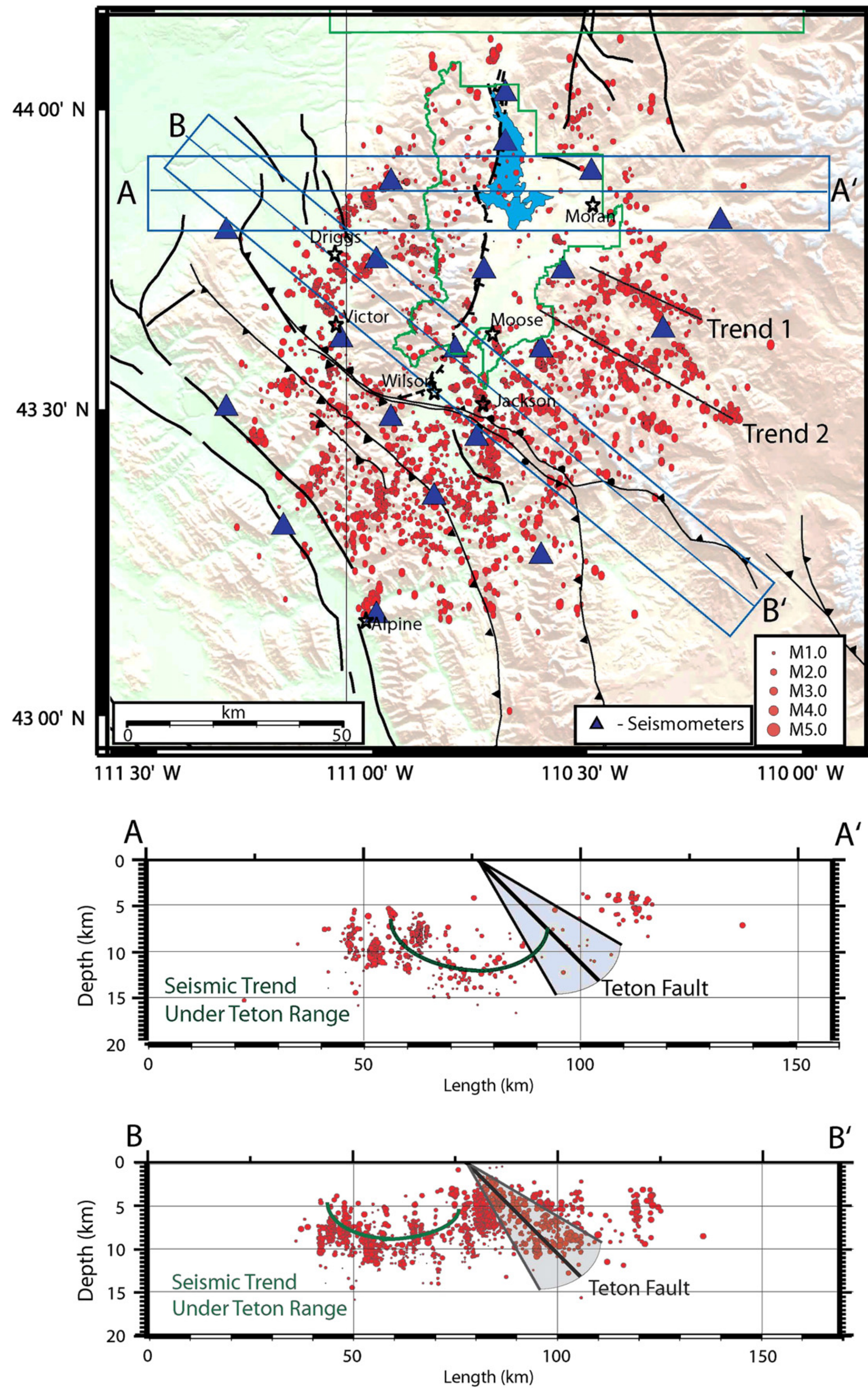

Fig. 6. Hypocenters of 8537 Teton earthquakes from 1986–2002 relocated in this project. Hypocenters are represented by red circles shown in both plain view and vertical depth view. The Teton fault is projected with an eastward dip of 30° to 60° ranges with a 45° dip outlined in black. Linear spatial trends in epicenter locations are labeled. Hypocenters plotted in the cross-section were only the A and B quality events that are well defined with epicentral errors less than 1 km, and vertical errors less than 5 km.

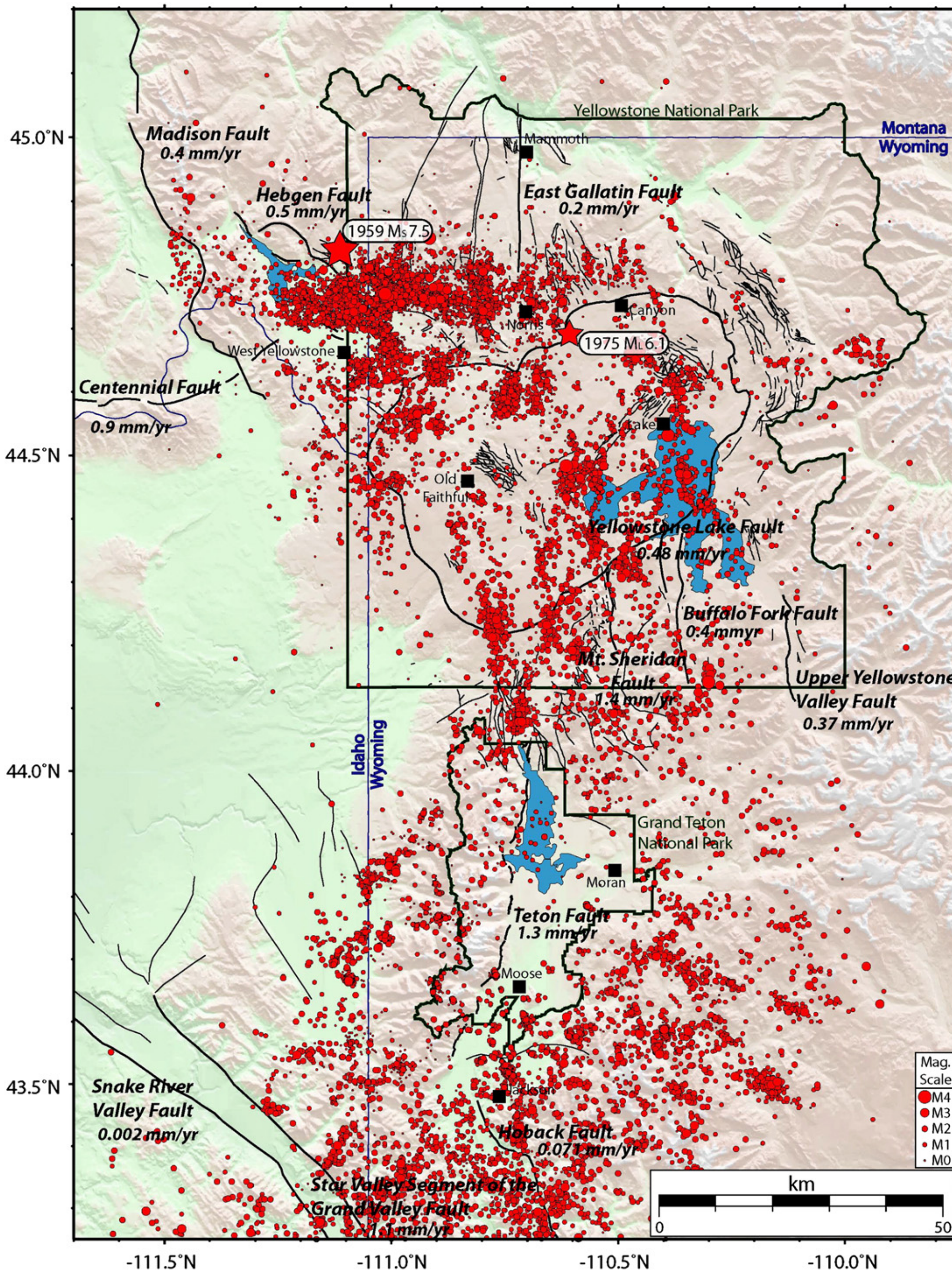

Fig. 7. Epicenters of the Teton–Yellowstone region from the combined 1986–2002 Teton–Yellowstone data set. Yellowstone data from Husen and Smith (2004).

Other notable observations are clusters of epicenters near the southern end of the Teton fault segment close to Jackson (Fig. 6). The Teton fault splays out into the southwest-dipping Jackson thrust, the northeast-dipping Cache Creek thrust sheet and the Hoback normal fault hanging and footwalls. These seismic trends could be associated with the Cache Creek thrust sheets, which could suggest that the Teton fault was part of a low-angle duplex suggested originally by Lageson (1992). Focal mechanisms in this area do show some support of low angle nodal planes along these trends.

We specifically note that there is little seismicity that can be directly attributed to activity along the Teton fault (Fig. 6). This observation is seen from the hypocenter cross-section AA′ across the Teton fault where there is no apparent alignment of hypocenters along the down-dip projections of the Teton fault for dips of 30° to 60° (Fig. 6). However, there are some hypocenters that show an apparent alignment along the fault dip in cross-section BB′ (Fig. 6). An interesting observation from these data is that the seismicity-band in the footwall displays a downward curved band of hypocenters beneath the Teton Range. We speculate that this pattern may outline the crystalline basement root of the range.

Alternately, the curved pattern could be related to flexure of the deforming footwall block caused by slip along the Teton fault that may be related to larger scale flexure into the Snake River Plain described by Janecke et al. (2000). During uplift of the Teton mountain block along the Teton normal fault, a rigid elastic beam-like structure would have the tendency to bend in the direction of the motion, which in this case would be vertically upward. This vertical motion could cause numerous small cracks and fractures to form in the footwall close to the faulting plane. This might also explain why hypocenters occur at shallow depths in the footwall close to the fault plane and then deepen to the west and increase in frequency below the roots of the Teton Range. However, we have not observed any compressional focal mechanisms along the top portion of this rigid beam structure with extensional mechanisms along the bottom.

In addition, the flexure of the Teton mountain block could in part be a result of the lithospheric downwarp of the Snake River Plain and Yellowstone volcanic hotspot track. Janecke (1995) hypothesized that the Teton fault is not a typical fault associated with the eastern Basin and Range but is the result of subsidence of the Snake River Plain caused by lithospheric cooling and a negative load imposed by a high density mid-crustal sill (DeNosaquo et al., 2009-this volume) resulting in back tilt of the Teton and Centennial mountain blocks westward and southward, respectively, into the subsiding SRP. It is likely that a combination of both processes have aided in effecting the stress regime of the Teton fault.

5. Stress Field for the Teton–Yellowstone Region

The combined stress field orientations for the study area are shown in Fig. 8. The Teton region shows that the average direction of the principal compressional stress axes of E–W is consistent with an E–W horizontal minimum stress associated with normal faulting trending N–S and thus suggests continuity of this stress regime since formation of the Teton block, ~ 10 to 5 Ma ago (Fig. 8). This stress field is typical of the Basin and Range Province.

However, in the northern part of the Teton fault zone, oblique–normal fault mechanisms exhibit a minimum principal stress oriented NE–SW. This anomalous orientation is interpreted as due to the influence of contemporary deformation, late Quaternary uplift and subsidence associated with the Yellowstone caldera (Pierce et al., 2007) that is only 20 km north of the northern end of the Teton fault as described by Hampel and Hetzel (2008). This suggests a possible explanation for the seismic quiescence along the Teton fault. Given the unique stress orientations around the northern Teton fault segment, the fault may be locked due to westward compression, which would also be loading the fault segment at the same time.

The effect of the Yellowstone hotspot swell on the Teton fault, and vice versa, has been also suggested by Smith et al. (1993). Similar conclusions were obtained in a finite element study by Hampel and Hetzel (2008) who modeled the high rates of Yellowstone caldera uplift and subsidence. They showed caldera deformation can induce variations of the stress field on the Teton fault including horizontal compression that is implied by the modern GPS observations (Puskas et al., 2007) described next.

The contemporary deformation of the Teton area and its relation to the overall strain field of the Yellowstone region was assessed by GPS observations of Puskas et al. (2007). The GPS field surveys from 1986 to 2000 indicate the unexpected result, namely that the valley of Jackson Hole is moving upward with respect to the Teton Mountain block and principal horizontal extensional strain axis is generally perpendicular to the fault. This observation implies crustal shortening and compression of the Jackson Hole Valley crust against the fault (Fig. 9). But more importantly the observed westward valley motion from the stations closest to the Teton fault supports the idea that the fault may be locked in compression.

During the period, 1987–1995, subsidence and contraction of the Yellowstone caldera only 15 km north of the Teton region was recorded during the same time as valley uplift and extension in the Gros Ventre Range implying that the Jackson Hole Valley block is moving toward the Teton fault (Puskas et al., 2007). During 1995–2000, uplift of the Yellowstone caldera GPS-derived ground motion vectors across the Jackson Hole Valley were directed west with almost 2 mm/yr of E–W motion, which was larger motion than detected from 1987–1995 (Puskas et al., 2007) (Fig. 9). This unusual stress state is consistent with the models of Hampel and Hetzel (2008) that suggested that the stress state may be due to the interaction of long-term uplift over the last 3000 yr (Pierce et al., 2007) of the Yellowstone caldera and imposed westward compression on the Teton fault. In our observations, the vertical strain, as measured at nearby stations on the opposite side of the Teton fault, is increasing stress on the fault since the vertical deformation rates are an order of magnitude greater than the horizontal rates.

The regional stress field of the Yellowstone area (Waite and Smith, 2004) was also computed from focal mechanisms of historic earthquakes, using the same methodology used in this study. Stress orientations in southern Yellowstone dominantly trend in an oblique northeastern minimum stress direction (Fig. 8). This unusual stress field may also reflect the systematic rotation of the extension from the E–W around the Teton fault to the NNE–SSW in northwestern Yellowstone and Hebgen Lake region. These results thus document the notable 90° rotation of the extensional stress regime from N–S northwest of the Yellowstone caldera in the Hebgen Lake earthquake area, rotating around the caldera to E–W on the Teton fault. This pronounced change in regional stress is interpreted by Smith et al. (2009-this volume) to be related to the interaction of Basin-Range extension locally effected by lithospheric buoyancy associated with volcanic processes of the Yellowstone hotspot.

6. Seismic hazard analysis

We now discuss a quantitative assessment of earthquake hazard by determining the frequency of earthquake occurrence and the coupled effect of strong ground shaking. In addition to fault slip-rate data, the combined and improved earthquake catalog for the Teton–Yellowstone region (Fig. 7) served as input into the probabilistic seismic hazard analysis (PSHA). The highest quality earthquake location data are most important to improve the characterization of background seismicity, which impacts the seismic hazard at shorter return periods (higher exceedance probabilities) or in areas more distant from the high slip-rate faults.

To model earthquake occurrence as a random process, the earthquake data had to approximate random space–time characteristics, e.g., foreshocks, aftershocks, and swarms had to be removed (declustered) while still retaining the largest earthquake in each swarm. Swarms were removed in the combined earthquake catalog for the Teton–Yellowstone region using the methodology of Waite (1999). A swarm is defined if the following two criteria were met: (1) the total number of earthquakes in a sequence is at least 20, and (2) the maximum of the daily number of events in the sequence is greater than twice the square-root of the swarm duration in days.

On this basis only five swarms were identified in the Teton earthquake catalog that fit the criteria defined by Waite (1999). In contrast, more than 50 swarms were identified in the Yellowstone region (also see the detailed earthquake swarm analysis for Yellowstone by Farrell et al., 2009-this volume). Once the swarms were removed, the reduced earthquake catalog was analyzed to identify foreshocks and aftershocks. This function was done using the program ZMAP (Wiemer and Zuniga, 1994), which removed aftershocks based on an algorithm by Reasenberg (1985). This algorithm identifies aftershocks by modeling an interaction zone around each earthquake. Based on this analysis, an additional 714 clusters of earthquakes of several hundred events were removed. Finally an analysis of the degree of completeness for the Teton–Yellowstone catalog for magnitudes was set to the lower cutoff of M_L 2.0, that yielded a cumulative frequency of occurrence, or b-value of 1.08 ± 0.05 and an a-value, or number of earthquakes per unit time of 2.1 (scaled to the annual frequency of earthquakes recorded in the JLSN).

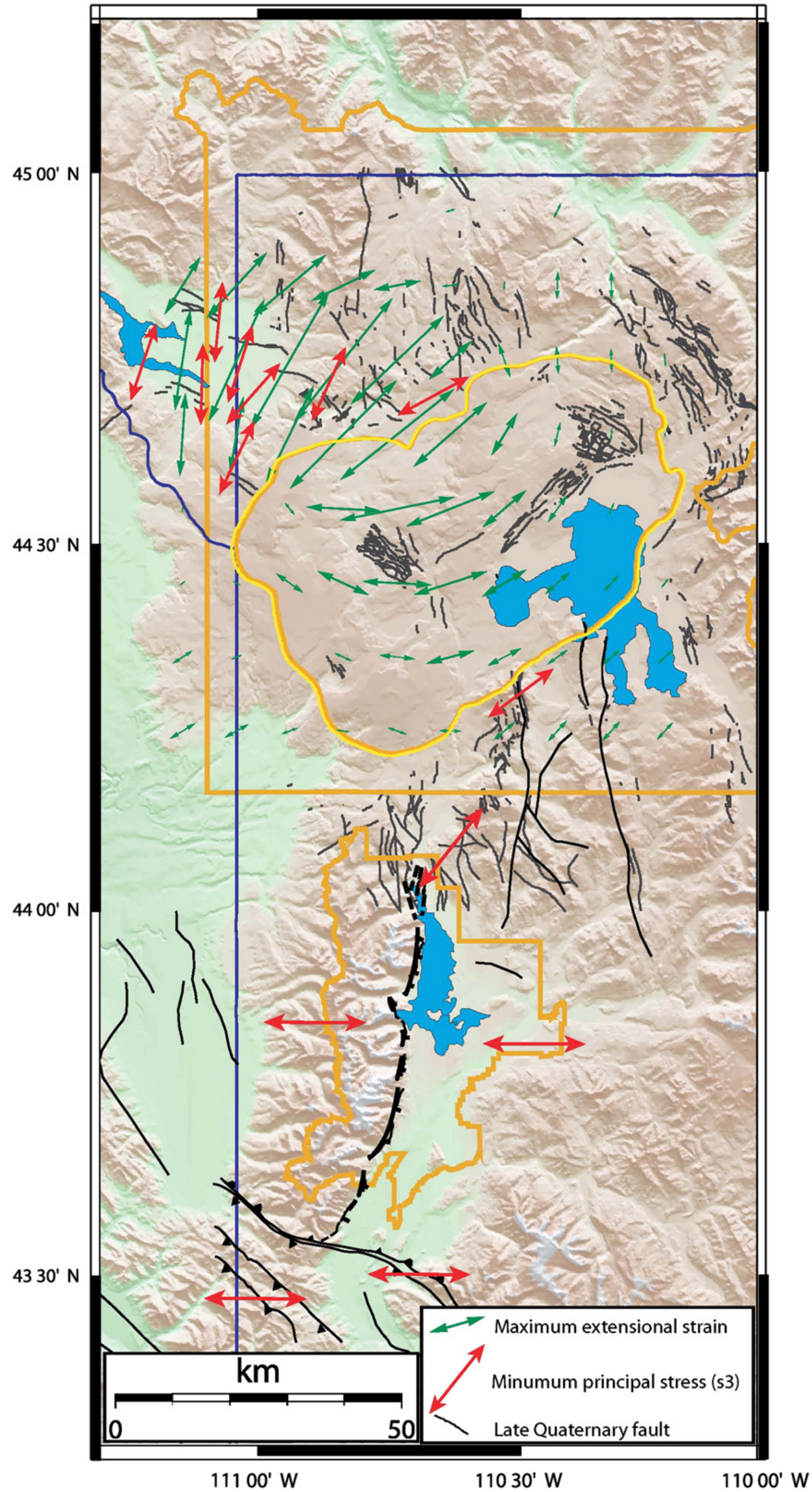

Fig. 8. Seismic and geodetic stress indicators for the Teton–Yellowstone region. The minimum principal stress-directions, σ_3, are shown by the red arrows determined from inverted focal mechanism data. Maximum extensional strain axes directions measured by GPS for 1995–2000 from Puskas et al. (2007) are represented by the green arrows and their lengths are proportional to the strain rate.

Earthquake recurrence rates for the Teton area are comparable to historic moment rates observed in other parts of the ISB, indicating that long-term seismicity in the Tetons is similar to that of the other regions. Large earthquakes ($6.5 < Mw < 7$) are estimated to occur in the Teton–Yellowstone region at about ~200 yr recurrence time (Doser and Smith, 1983).

For the long-term fault slip rates we included data from the Teton fault and additional 12 major faults in the Teton–Yellowstone region for the hazard calculation (Fig. 7). Parameters, including slip rates, for these major Quaternary faults were taken from the USGS Fault and Fold Database (Table 3 and USGS-WY, 2006; USGS-MT, 2006; USGS-ID, 2006). For the Quaternary faults with various slip rates an alternate table

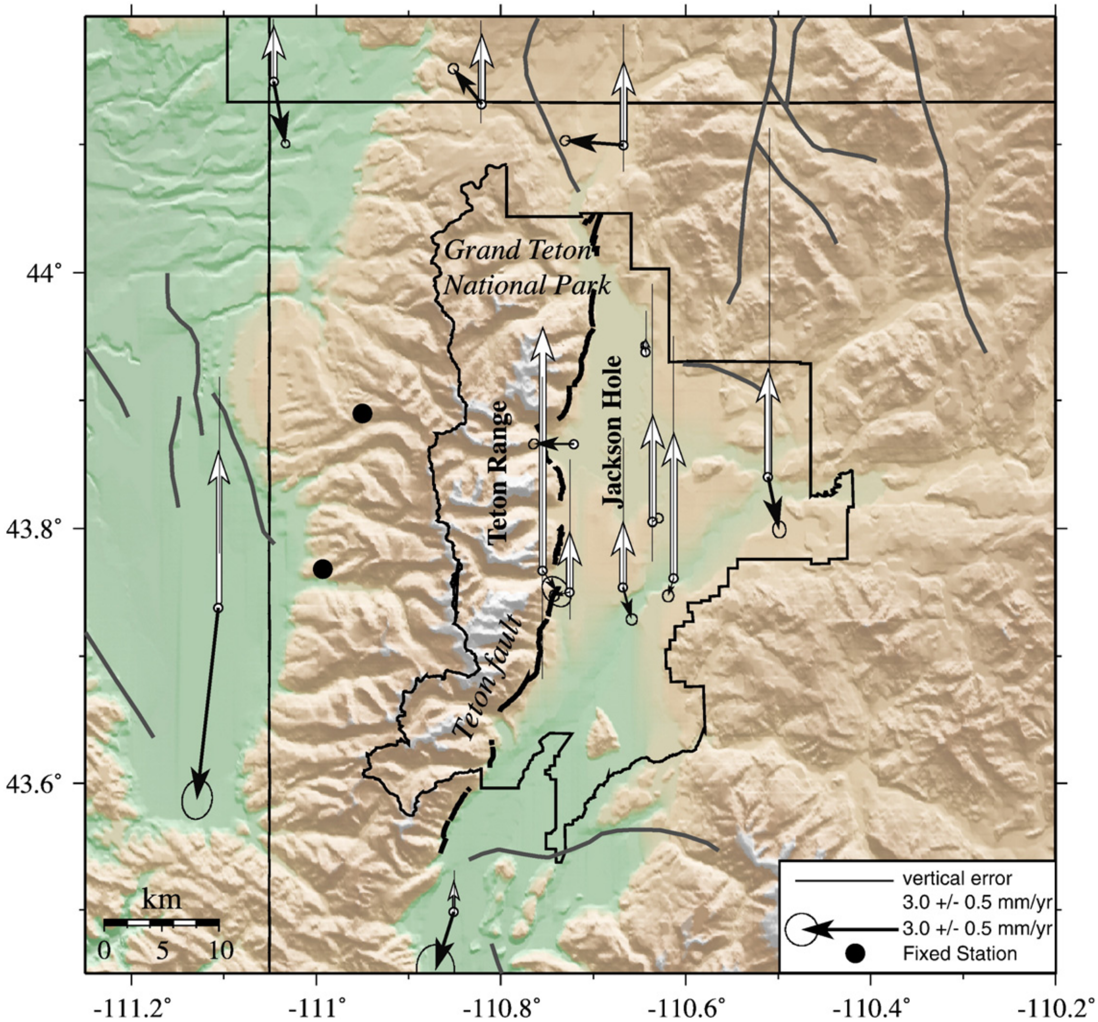

Fig. 9. GPS-derived ground motion vectors for the Teton region from 1996–2002 (after Puskas et al., 2007). White arrows indicate vertical motion and black arrows indicate horizontal motion that demonstrates a westward motion of the crust against the Teton fault. Note the larger uplift of the Teton Range compared to the Jackson Hole Valley.

of slip rates is in the supplemental section (Table S1). The faults with the highest rates in the study region included the Teton, Mt. Sheridan, Hebgen Lake, Madison, Gallatin and Yellowstone Lake faults (Fig. 7).

For the Teton fault slip-rate we used estimates of post-glacial offset based on fault offset that was measured from the fault height corrected for hanging wall backtilt in a glacial moraine at Granite Canyon, southern Teton Range (Smith et al., 1990; Byrd et al., 1994). This is the only trench on the Teton fault and provides direct information on the most recent fault slip. An age of the glacial moraine of ~14,000 yr was assumed (Licciardi and Pierce, 2008). The trench data revealed two paleoearthquakes: 1) the oldest at ~7980 yr ago with a 2.8 m offset, and 2) the youngest of a 1.3 m displacement event that occurred ~4800 yr ago (Smith et al., 1990: Byrd et al., 1994). This is a key observation because it suggests a 5 ka hiatus since the last major rupture of over a meter of displacement of the Teton fault, implying a protracted period of relatively low rate of fault-loading to the present. But more importantly, the dated ~4 m of offset from the trench data requires that the 10 m offset of the total ~14 m fault offset at the Granite Creek, had to occur in the 6 ka period prior to the oldest trenched event, implying a much higher slip rate from 14 ka to ~8 ka.

The cumulative fault offsets for the Teton fault with ages are plotted in Fig. 10 to evaluate the slip rates assuming a linear loading rate. From these data, the 10 m, oldest period of offset requires multiple large earthquakes such as five paloevents of magnitude Mw ~7 (estimated from Wells and Coppersmith, 1994), with a frequency of occurrence of ~1000 yr. This implies a higher level of seismicity than evidenced by the historic record. These data also suggest that the fault slip rates were notably lower during the later Holocene (last 5000 yr) period to the present. This makes the assignment of fault slip rate problematical in a PSHA.

These large differences in prehistoric slip rates could be related to glacial unloading of the mountain ranges as proposed by Hampel and Hetzel (2006). Similar to the Teton fault, the Wasatch fault and three adjacent normal faults in the Basin and Range have documented geologic and paleoseimological data that marks an increase in slip rates in lowering of Lake Bonneville faulting offsets relative to current measured slip rates Hetzel and Hampel (2005). Hampel et al. (2007) used lithospheric flexure models to conclude that fault activity is expected to be concentrated at times of glacial loading and unloading associated with the Yellowstone glacial mass (1 km thick). We acknowledge that this could be a contributing factor; however, Hampel and Hetzel (2008) also argue for uplift and deformation of the caldera and favored the caldera-fault interaction as the key mechanism for contributing to the fault slip rate. We have noted that the measured fault slip rate takes into account the entire post glacial offset history, so implicitly it contains the effect of all uplift mechanisms.

In Fig. 10, the estimated slip rates from 14,000, glacial retreat, to ~8000 yr ago gives a value of 2 mm/yr slip rate; however, the post 8000 yr values are much smaller, 0.16 mm/yr. These observations point out the dilemma of which value to employ in a PSHA determination. For standardization we choose to use the long-term slip rate assigned in the USGS Fold and Fault Database for the Teton fault of

Table 3
Slip rates of the faults used in the PSHA study of the Teton–Yellowstone region.

Fault name	Faulting type	Average slip-rate
Teton Fault	Normal	1.3 mm/yr
Hoback Fault	Normal	0.071 mm/yr
Star Valley Segment of the Grand Valley Fault	Normal	1.1 mm/yr
Snake River Valley Fault	Normal	0.002 mm/yr
Mount Sheridan Fault	Normal	1.4 mm/yr
Buffalo Fork Fault	Normal	0.4 mm/yr
Upper Yellowstone Valley Fault	Normal	0.37 mm/yr
Yellowstone Lake Fault	Normal	0.48 mm/yr
Centennial Fault	Normal	0.9 mm/yr
Hebgen Fault	Normal	0.5 mm/yr
Madison Fault	Normal	0.4 mm/yr
East Gallatin Fault	Normal	0.2 mm/yr

Data has been taken from the USGS Fault and Fold Database (USGS-WY, 2006; USGS-MT, 2006; USGS-ID, 2006).

1.3 mm/yr for the hazard calculation (Fig. 10), which is about the average of our above rates. Also Fig. 10 shows a key aspect of the Teton earthquake hazard namely that there may be currently a slip deficit of ~2 m, implying there is sufficient stored energy for a release in a magnitude Mw7 earthquake.

In the Yellowstone Plateau, the shallow thickness of the seismogenic zone associated with very high temperatures that inhibit brittle fracture beneath the Yellowstone caldera and restricts faulting to ~4–6 km depth with lengths no greater than those of the resurgent-dome; graben faults of a few tens of kilometers (Waite and Smith, 2004). Volcanic earthquakes are of course a possibility, but they seldom exceed magnitude Mw 6.5 in other areas of the world including the Snake River Plain (Smith et al., 1996). For earthquakes directly associated with dike intrusion, the maximum magnitudes are estimated to be ~Mw 5. For the Yellowstone caldera the maximum magnitude earthquake of Mw 6.5 was used based on fault lengths and depths (width) of the seismogenic zone (Wells and Coppersmith, 1994). The magmatic-related faults of Yellowstone are considered seismogenic at the magnitude threshold of Mw 6.5+, but they can produce volcanic seismic activity of smaller magnitude earthquakes (Waite and Smith, 2004).

Modern earthquake data including recurrence rates from the new Teton–Yellowstone historic data described above provided the parameters for the background seismicity. The PSHA code HAZ38_2006 employed in our study was developed by Abrahamson (2006). This code determines peak ground acceleration (PGA) and spectral accelerations as a function of annual exceedance frequency or return period. In our study we restricted our hazard calculation to the peak ground accelerations as that value is more easily understood by the user geology and emergency management personnel. We also employed the ground motion attenuation relationship by Spudich et al. (1999), which is generally accepted for western U.S. extensional tectonic regimes of the Basin and Range Province, and thus applicable to the Teton–Yellowstone region, in our PSHA ground accelerations determinations.

We note that our PSHA results are preliminary because the results are for general rock site conditions they do not account for the effects of the near-surface soils and characterizations of the local site geology that are necessary to produce site-specific hazard assessment but for which such information is not available for the Teton–Yellowstone region. Thus our results should only be used as a first-order estimate at the relative seismic hazard of the region and should only be used for guidance of land use and building planning

The characterizations of the seismic sources for the Teton–Yellowstone region have well documented uncertainties in the input parameters (White, 2006). In HAZ38_2006, the epistemic uncertainties of the seismic sources are incorporated in the analysis via a logic tree

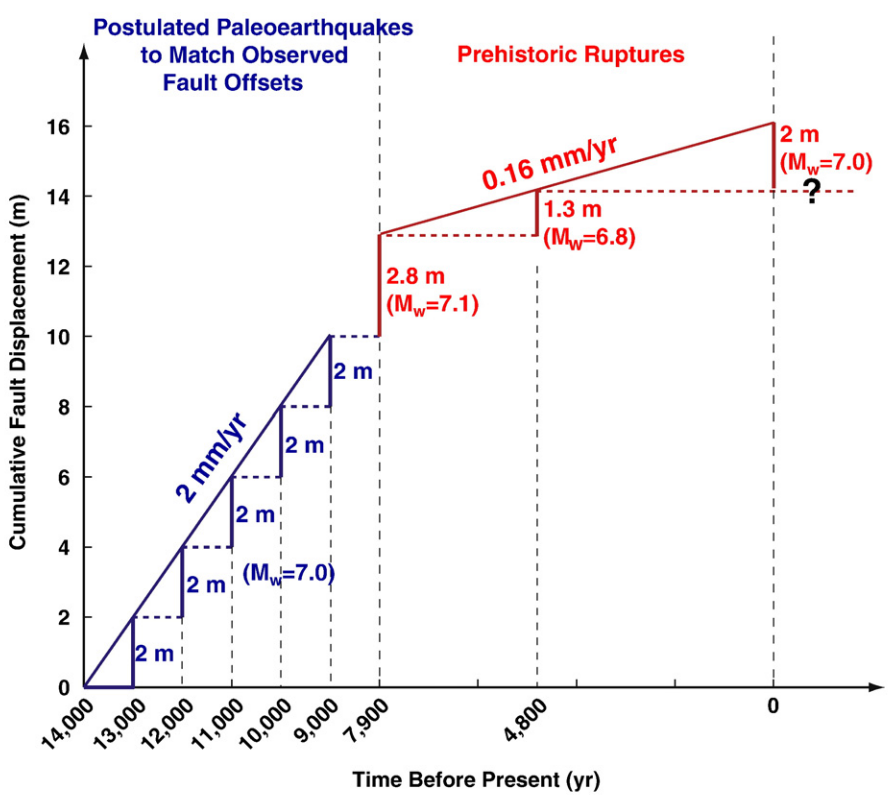

Fig. 10. Paleoearthquake Teton fault slip rates. The figure shows the fault slip rate estimates for the Teton fault using postulated paleoearthquakes that would have been necessary in order to account for the observed fault offsets along the Teton fault scarp (in blue), and the prehistoric ruptures determined from the trenching results (in red). The youngest recorded prehistoric rupture was a M6.8 earthquake 4700 to 6000 yr ago that generated a 1.3 meter offset. The next youngest rupture was a M7.1 earthquake 7300 yr ago that generated a 2.8 m offset. Using the prehistoric ruptures a fault loading rate of 0.16 mm/yr is calculated and extrapolated to the present time to estimate the next possible rupture on the Teton fault (Byrd et al., 1994).

approach, allowing the user to specify multiple possible values for each of the parameters used to characterize the fault behavior and to assign discrete probabilities or weights to each of these values or models. Aleatory uncertainty also is accounted for in this code by defining probability density functions for the earthquake magnitude, location, and rupture dimensions.

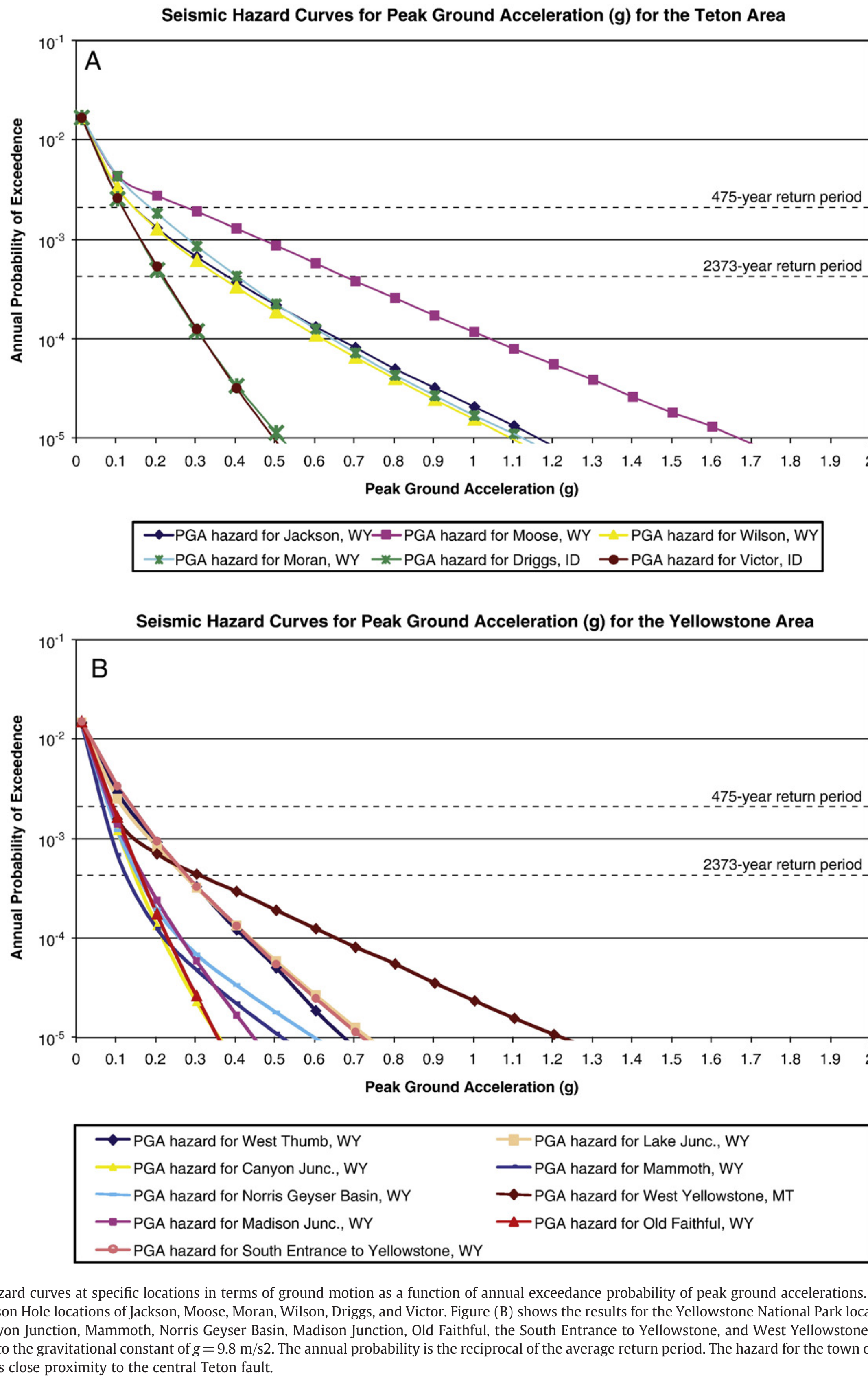

Fig. 11. Seismic hazard curves at specific locations in terms of ground motion as a function of annual exceedance probability of peak ground accelerations. Figure (A) shows the results for the Jackson Hole locations of Jackson, Moose, Moran, Wilson, Driggs, and Victor. Figure (B) shows the results for the Yellowstone National Park locations of West Thumb, Lake Junction, Canyon Junction, Mammoth, Norris Geyser Basin, Madison Junction, Old Faithful, the South Entrance to Yellowstone, and West Yellowstone, Montana. The *x*-axis values are relative to the gravitational constant of $g = 9.8$ m/s2. The annual probability is the reciprocal of the average return period. The hazard for the town of Moose, Wyoming, is the largest given its close proximity to the central Teton fault.

7. Seismic hazard of the Teton–Yellowstone region

The probabilistic hazard was calculated at 15 specific key locations in the Teton–Yellowstone region including the towns of Jackson, Moose, Moran, and Wilson, Wyoming. Sites in Yellowstone included West Thumb, Lake Junction, Canyon Junction, Mammoth, Norris Geyser Basin, Madison Junction, Old Faithful, the South Entrance to Yellowstone and for the town of West Yellowstone, Montana. We calculated hazard on the west side of the Teton Range at Driggs and Victor, Idaho. The hazard curves for PGA for each site are shown in Fig. 11. The largest PGA for average return interval of 1000 yr is about 0.5 g for the town of Moose, Wyoming located in the Jackson Hole Valley. The hazard curves for the other towns of Jackson, Moran, Wilson, Driggs, and Victor have lower PGA exceedance values of about 0.3 g for a 1000-year return period (Fig. 11).

In addition, we made hazard estimates for the variable slip rates on the Teton fault and other slip rate variations from faults used in the PSHA (Table S1). The results are shown in the supplemental section (Figs. S1 and S2). For the 8 ka, youngest period, a slip-rate value of 0.16 mm/yr for the Teton fault was employed. This lower rate markedly reduces the peak ground acceleration values near the Teton fault at Moose, WY by ~30%. These lower slip rate results are plotted for comparison as a dashed line on the earthquake hazard curves for sites most affected by the Teton fault and in a regional map view in Fig. S2. Other slip rate changes for the major Quaternary faults included the Star Valley segment of the Grand Fork fault, Buffalo Fork fault, Yellowstone Lake fault, and the East Gallatin fault based on the work of Machette et al. (2001). Variations of the Centennial fault were determined by Petrick (2008) and Ruleman (2002) for the Madison fault. These supplemental slip rates changed the overall PSHA results for our locations by less than 1%.

In a final step, preliminary PSHA maps were produced using HAZ38_2006 for gridded sources every 0.1° from northern Yellowstone and the Teton region. The maps were determined for return periods of 500, 1000, and 2500 yrs (Fig. 12 A–C). Within the different return periods, the highest hazards in the mapped areas are typically the same, i.e., Jackson Hole Valley and the southeastern portion of Yellowstone National Park. The hazard in the Teton–Yellowstone region is dominantly controlled by the faults with the highest recorded slip rates. The Teton fault dominates the hazard along with the Buffalo Fork, Mt. Sheridan, Yellowstone Lake and Yellowstone River Valley faults. Other faults such as the Grand Valley, Snake River, and Centennial faults also contribute to a higher hazard in the 2500 year return period that is of the order of the recurrence intervals of late Quaternary faulting (Fig. 12C).

We note that time-variable fault slip rates are problematical and the incorporation of such data uncertainties should be carefully evaluated in hazard assessment as we suggested for the two slip rates noted for the post-glacial offset of the Teton fault. For example submerged shorelines of the Jackson Lake near the north end of the Teton fault suggests two periods of post-glacial subsidence that may have been associated with earthquakes (Pierce et al., 2003).

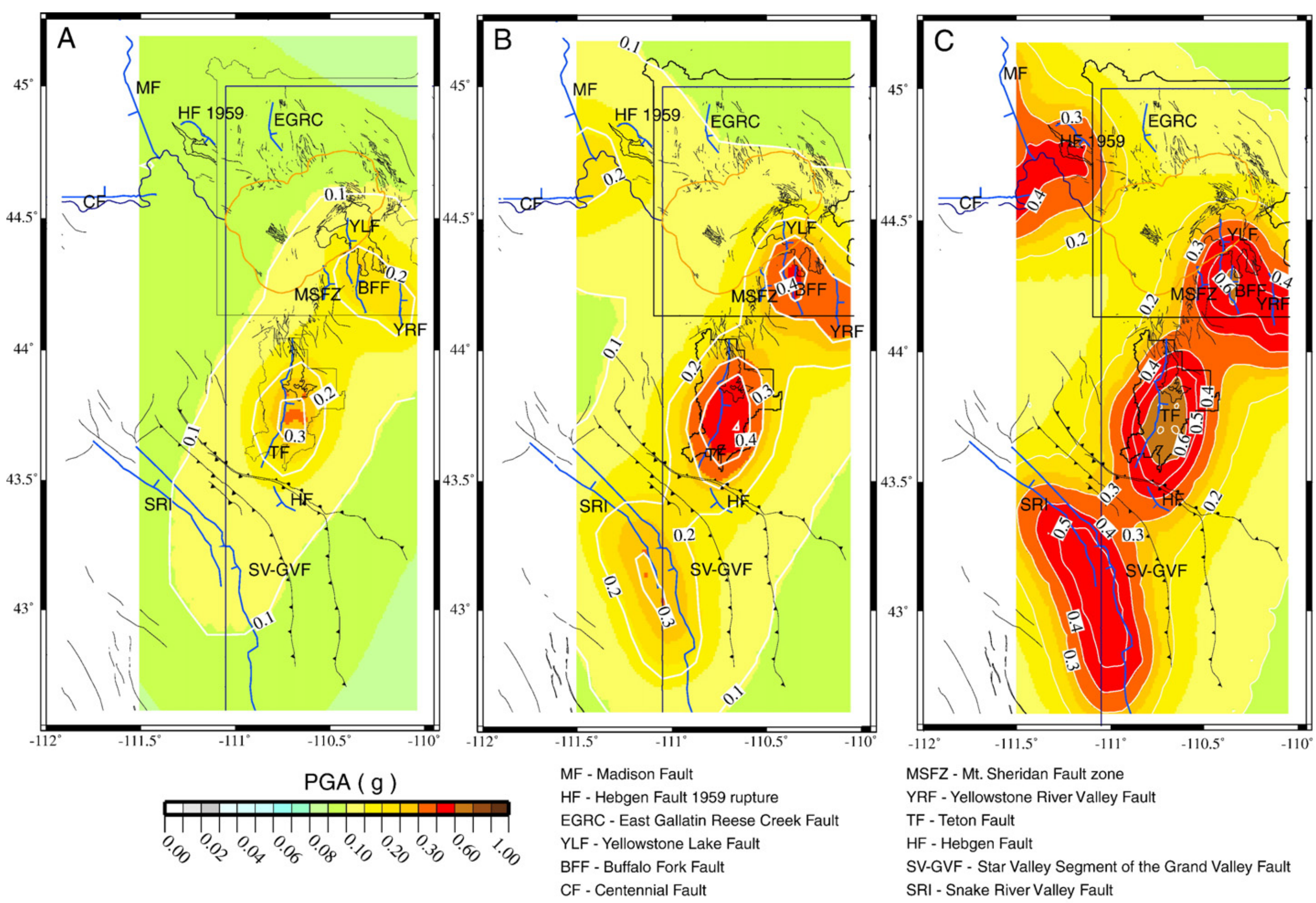

Fig. 12. A) Probabilistic seismic hazard analyses (PSHA) maps of the greater Teton–Yellowstone region for peak ground accelerations (PGA) with a 10% probability of exceedance in 50 yr (~500 yr). The color scale is based on PGA values relative to the gravitational constant of $g = 9.8$ m/s2. The blue colored faults had the largest slip-rates of any faults in the area and were used in the PSHA calculation. The small blue lines perpendicular to each fault show the fault's normal faulting dipping direction. The minor area faults shown in gray were not included in the PSHA. The PGA contours are outlined in white, B) same as A) but for 5% probability of exceedance in 50 yr (~1000 yr), C) same as B) but for PGA with 2% probability of exceedance in 50 yr (~2500 yr).

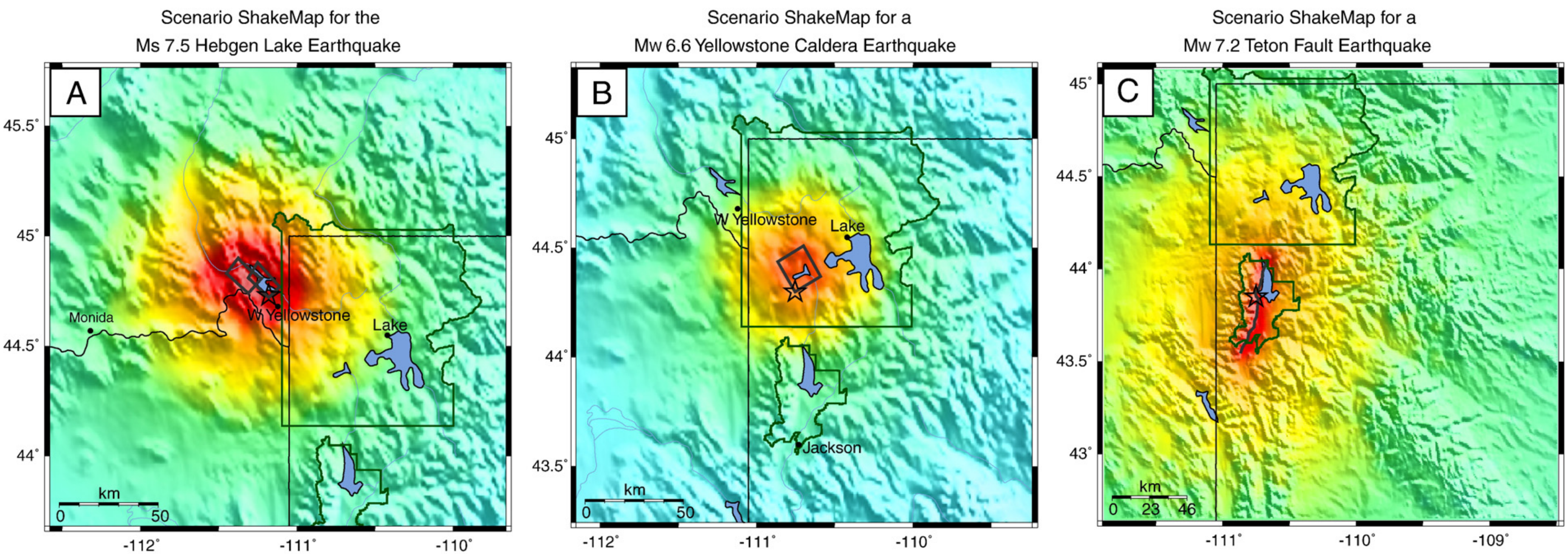

PERCEIVED SHAKING	Not felt	Weak	Light	Moderate	Strong	Very strong	Severe	Violent	Extreme
POTENTIAL DAMAGE	none	none	none	Very light	Light	Moderate	Moderate/Heavy	Heavy	Very Heavy
PEAK ACC.(%g)	<.17	.17-1.4	1.4-3.9	3.9-9.2	9.2-18	18-34	34-65	65-124	>124
PEAK VEL.(cm/s)	<0.1	0.1-1.1	1.1-3.4	3.4-8.1	8.1-16	16-31	31-60	60-116	>116
INSTRUMENTAL INTENSITY	I	II-III	IV	V	VI	VII	VIII	IX	X+

Fig. 13. Scenario ground shaking (ShakeMaps) of large earthquakes in the Teton–Yellowstone region, including: A) the Ms 7.5 1959 Hebgen Lake, MT, earthquake; B) a scenario Mw 6.6 on a normal fault on the Mallard Lake resurgent dome, and C) a scenario Mw 7.2 earthquake on the Teton fault. Ground shaking on the maps is shown for the expected peak ground acceleration, peak velocity and instrumental intensity (Wald et al., 2003).

Pierce et al. (2003, 2007) consider subsidence to be due to release of hydrothermal fluids by any mechanism such as rupture of a hydrothermal seal due to fluid pressure buildup, to cracking associated with a local earthquake of more distant earthquake, perhaps on the Teton fault. If these features can be accurately dated and parameterized in terms of offset on the Teton fault, this information can be incorporated into a new hazard determination. Also new research on implementation of GPS-determined fault loading rates may also be used in the future.

We conclude our study of earthquake hazards of the Teton–Yellowstone region by showing maps of potential ground shaking for large earthquake scenarios in the region. These "ShakeMaps" (Wald et al., 2003) are model representations of ground shaking expected by a scenario earthquake. They can be created as actual real-time hazard maps immediately following a large earthquake that can be used by emergency responders to evaluate the distribution of ground shaking for first-response purposes. The ground shaking levels shown on ShakeMaps depends on the earthquake rupture process, the distance from the earthquake source, the rock and soil conditions at the site, and effects on the propagation of seismic waves from the earthquake due to complexities in the structure of the Earth's crust called attenuation.

Scenario ShakeMaps for the Teton–Yellowstone region (Fig. 13) were produced by David Wald of the USGS (http://earthquake.usgs.gov/eqcenter/shakemap/list.php?y=2008) and include the following events: 1) the 1959 Ms 7.5 Hebgen Lake earthquake, 2) a non-scarp-forming Mw 6.6 event associated with a normal fault on the Mallard Lake resurgent dome, and 3) a Mw 7.2 earthquake on the Teton fault.

The scenario 1959 Ms 7.5 Hebgen Lake earthquake ShakeMap (Fig. 13A) reveal violent to extreme ground motions extending 50 km from the fault rupture. This pattern of ground shaking is consistent with the areas of observed extensive damage and changes in hydrothermal features of Yellowstone (Christiansen et al., 2007).

As an example of the largest expected earthquake within the Yellowstone caldera, an Mw 6.6 earthquake was simulated on a normal fault on the Mallard Lake resurgent dome graben (Fig. 13B). This scenario event is important to the Yellowstone area as thousands of tourists visit the Upper Geyser Basin daily during the summer. Ground shaking for this event could be caused by an earthquake that would not rupture to break the surface, i.e., it would be a non-scarp forming event. Nonetheless, ground shaking could be strong to very strong in the vicinity of the event and it be would be widely felt throughout Yellowstone National Park. An earthquake of this magnitude could lead to moderate to severe damage to structures not built to modern earthquake design standards.

A final scenario (Fig. 13C) is for a Mw 7.2 earthquake on the Teton fault that would rupture the entire 55 km length of the fault. In this scenario, violent to extreme ground shaking would occur within ~10 km of the fault. The valley of Jackson Hole would experience violent to very strong shaking that could produce heavy damage to structures not built to seismic standards.

8. Concluding remarks

Earthquake data from the Jackson Lake seismic network were used to produce a new higher accuracy earthquake catalog for the Teton region employing a tomographic 3-D V_P model of the upper and mid-crustal structure. The Teton fault has displayed little seismic activity along mainly the northern and middle segments, which exhibits the greatest and most recent prehistoric displacement. Whether this observation is due to the possible episodic nature of seismicity along the segments or other factors is not known, but the possibility that this segment is locked and storing strain energy is a certainty.

Tomographic images of the Teton region revealed velocity structures that separate the footwall from the hanging wall of the Teton normal fault, but did not aid in determining the actual dip angle of the fault itself. However, basin structures and deeper bedrock structures were resolved to 12 km depth. Focal mechanisms provided data for stress field inversions that indicated dominant E–W extension in the southern and central Teton fault segments but with an unexpected change to NE–SW extension in the northern segment dominated by the Yellowstone Plateau volcanic system.

The new high precision Teton earthquake data was combined with the results of a comparable study of the 3-D velocity structure and a new catalog of highest precision hypocenters of Yellowstone earthquakes by Husen and Smith (2004). The combined data provide the most accurate hypocenter locations and magnitudes were then employed with data on late Quaternary fault-slip rates in a preliminary earthquake hazard assessment.

Although the PSHA data for the Teton–Yellowstone region did not incorporate local site effects and are thus a general guide to earthquake hazard, the PSHA data shows that the highest seismic hazard is in the Jackson Hole Valley and is associated with the Teton fault. In Yellowstone the highest hazards are related to large faults that extend as right-stepping structures from the Teton fault in the southern part of Yellowstone National Park along the East Sheridan fault zone.

Our earthquake hazards assessment of the Teton–Yellowstone region demonstrates that the hazard is dominated by the late Quaternary faults of the Yellowstone hotspot that affects a large area of Wyoming, Idaho and Montana. We note that our results are similar to the USGS National Hazard Maps (Petersen et al., 2008) that show similar areas of pronounced seismic hazard as determined in this study. However, our analysis is a separate and independent assessment of the earthquake hazard using a different algorithm including both epistemic and aleatory uncertainties as compared to the methodology used by the USGS. The PSHA requires high-quality reliable earthquake data that was not available for the Teton region until our determination of the highest quality catalog of hypocenters with unified magnitudes. The new earthquake locations are most important to improve the characterization of background seismicity, which impacts the hazard at shorter return periods (higher exceedance probabilities) or in areas more distant from the high slip-rate faults. However, the overall hazard calculation is mainly driven by the late Quaternary slip rates of the large faults in the region therefore our results are similar to the USGS seismic hazard maps on a regional scale.

In summary, earthquakes can produce very significant hazards that can affect large areas of the Teton–Yellowstone region. This is particularly important because of the large number of visitors and residents in these national parks, especially during summer months. The earthquake hazards and risk must be taken into account by land use managers and planners for assessing the public safety that these hazards pose. We specifically note that our probabilistic hazard assessments are only a general guide to ground shaking and that studies of the surficial geology has to incorporate local site response effects in the ground motion hazard. We conclude by stating that the geologic hazards of the Teton–Yellowstone region include the effects of volcanic and hydrothermal features. This subject has been addressed in a preliminary volcano hazard assessment by Christiansen et al. (2007). Data from that study and from this hazard analysis should be combined to do a more complete, joint earthquake–volcano hazard assessment including the effects of time-dependent stress effects of earthquakes on volcanoes and vice versa.

Acknowledgments

Discussions with Dan O'Connell, Chris Wood and Lisa Block greatly helped with accessing the U.S. Bureau of Reclamation seismic data for the Teton region. Jim Pechmann provided insight into magnitude calibration and insight into the focal mechanism inversion was provided by Greg Waite. We also want to thank Charlotte Rowe, Christine Puskas, Art Sylvester, Tim Ahern, Norm Abrahamson, and Nick Gregor for their help with the geodetic data, and PSHA codes. Michael Jordan, Wu-Lung Chang, Aaron DeNosaquo, and Katrina DeNosaquo provided insight and assisted with computational and database aspects of the project. Support for the project was in part provided by the USGS NEHRP #05HQGR0026. The University of Utah Department of Geology and Geophysics provided fellowship funds and computational support. We would also like to thank the JVGR Reviewers for their advice.

Appendix A. Supplementary data

Supplementary data associated with this article can be found, in the online version, at doi: 10.1016/j.jvolgeores.2009.08.015.

References

Abers, G.A., Gephart, J.W., 2001. Direct inversion of earthquake first motions for both the stress tensor and focal mechanisms and application to southern California. J. Geophys. Res. 106 (B11), 26523–26540.

Abrahamson, N., 2006. HAZ38_2006, Pacific Gas & Electric. Personal communication, Spring, 2006.

Aki, K., Richards, P.G., 1980. Quantitative seismology. W.H. Freeman, New York.

Anders, M.H., Sleep, N.H., 1985. Lithospheric strengthening by magmatic intrusion: thermal and mechanical effects of the Yellowstone hotspot. J. Geophys. Res. 97, 15379–15394.

Anders, M.H., Geissman, J.W., Piety, L.A., Sullivan, J.T., 1989. Parabolic distribution of circumeastern Snake River Plain seismicity and latest Quaternary faulting: migratory pattern and association with the Yellowstone hotspot. J. Geophys. Res. 94, 1589–1621.

Barnosky, A.D., 1984. The Colter Formation: evidence for Miocene volcanism in Jackson Hole, Teton County, Wyoming, Wy. Geol. Assoc. Earth Sci. Bull. 16, 50–101.

Byrd, J. O. D., 1994, Neotectonics of the Teton fault, Wyoming, PhD dissertation, University of Utah, Salt Lake City, Utah, 295 pp.

Byrd, J.O.D., Smith, R.B., Geissman, J.W., 1994. The Teton fault, Wyoming: topographic signature, neotectonics and mechanism of deformation. J. Geophys. Res. 99, 20122–20140.

Christiansen, R.L., Lowenstern, J.B., Smith, R.B., Heasler, H., Morgan, L.A., Nathenson, M., Mastin, L.G., Muffler, L.J.P., Robinson, J.E., 2007. Preliminary assessment of volcanic and hydrothermal hazards in Yellowstone National Park and Vicinity. U.S. Geological Survey Open-File Report 2007-1071.

DeNosaquo, K., Smith, R.B., Lowry, A.R., 2009. Density and lithospheric strength models of the Yellowstone–Snake River Plain volcanic system from gravity and heat flow data. J. Volcanol. Geotherm. Res. 188, 108–127.

Doser, D.L., Smith, R.B., 1983. Seismicity of the Teton–southern Yellowstone region Wyoming. Bull. Seismol. Soc. Am. 73, 1369–1494.

Eberhart-Phillips, D., 1990. Three-dimensional P and S velocity structure in the Coalinga Region California. J. Geophys. Res. 95, 15343–15363.

Gilbert, J.D., Ostenaa, D., Wood, C., 1983. Seismotectonic study Jackson Lake Dam and Reservoir, Minidoka Project, Idaho–Wyoming. Bureau of Reclamation Seismotectonic Report, vol. 83–8, p. 123.

Farrell, J.M., Smith, R.B., Husen, S., 2009. Earthquake swarm identification and b-value mapping of the Yellowstone volcanic–tectonic system. J. Volcanol. Geotherm. Res 188, 260–276.

Hampel, A., Hetzel, R., 2006. Response to normal faults to glacial–interglacial fluctuations of ice and water masses on the Earth's surface, vol. 111. JGR. p13 p.

Hampel, A., Hetzel, R., 2008. Slip reversals on active normal faults related to the inflation and deflation of magma chambers: numerical modeling with application to the Yellowstone–Teton region. Geophys. Res. Lett. 35, L07301.

Hampel, A., Hetzel, R., Densmore, A.L, 2007. Postglacial slip-rate increase on the Teton normal fault, northern Basin and Range, caused by melting of the Yellowstone ice cap and deglaciation of the Teton Range. Geology 1007–1110.

Haslinger, F., Kissling, E., 2001. Investigating effects of 3-D ray tracing methods in local earthquake tomography. Phys. Earth Planet. Inter. 123, 103–114.

Hetzel, R., Hampel, A., 2005. Slip rate variations on normal faults during glacial–interglacial changes in surface loads. Nature 435, 81–84.

Husen, S., Smith, R.B., 2004. Probabilistic earthquake relocation in three dimensional velocity models for the Yellowstone National Park Region, Wyoming. Bull. Seismol. Soc. Am. 94, 880–896.

Husen, S., Smith, R.B., Waite, G., 2004. Evidence for gas and magmatic sources beneath the Yellowstone volcanic field from seismic tomographic imaging. J. Volcanol. Geotherm. Res. 131, 397–410.

Janecke, S.U., 1995. Eocene to Oligocene half grabens of east-central Idaho: structure, stratigraphy, age, and tectonics. Northwest Geol. 24, 159–199.

Janecke, S.U., Perkins, M.E., Smith, R.B., 2000. Normal fault patterns around the Yellowstone hotspot: a new model, abs. Geol. Soc. America Annual Meeting Program, Summit 2000, A45.

King, J.J., Doyle, T.E., Jackson, S.M., 1987. Seismicity of the eastern Snake River Plain region, Idaho, prior to the Borah Peak, Idaho, earthquake: October 1972–October 1983. Bull. Seismol. Soc. Am. 77, 809–818.

Kissling, E., 1988. Geotomography with local earthquake data. Rev. Geophys. 26, 659–698.

Kissling, E., Ellsworth, W.L., Eberhart-Phillips, D., Kradolfer, U., 1994. Initial reference models in local earthquake tomography. J. Geophys. Res. 99, 19635–19646.

Lageson, D.R., 1992. Laramide influence on the Teton normal fault, western Wyoming, in regional geology of Eastern Idaho and Western Wyoming. In: Link, P.K., Kuntz, M.A., Platt, L.B. (Eds.), Mem. Geol. Soc. Am., vol. 179, pp. 183–195.

Leopold, E.B., Lu, G., Love, J.D., Love, D.W., 2007. Plio-Pleistocene climatic transition and the lifting of the Teton Range, Wyoming. Quat. Res. 67 (1), 1–11.

Licciardi, J.M., Pierce, K.L., 2008. Cosmogenic exposure-age chronologies of Pinedale and Bull Lake glaciations in greater Yellowstone and the Teton Range USA. Quat. Sci. Rev. 27, 814–831. doi:10.1016/j.quascirev.2007.12.005.

Lomax, A., Virieux, J., Volant, P., Thierry-Berge, C., 2000. 101–134 pp. Probabilistic earthquake location in 3D and layered models. Advances in seismic event location. Kluwer Acad, Norwell, Mass.

Love, J.D., 1977. Summary of Upper Cretaceous and Cenozoic stratigraphy, and of tectonic and glacial events in Jackson Hole, northwestern Wyoming. Guide. Wyo. Geol. Assoc. Annu. Field Conf., 29th, pp. 585–593.

Love, J. D., Reed Jr., J. C., Christiansen, A. C., 1992. Geologic map of Grand Teton National Park, Teton County, Wyoming, scale 1:62,500, U.S. Geol. Surv. Misc. Invest. Ser., Map I-2031.

Love, J.D., Reed Jr., J.C., Pierce, K.L., 2007. Creation of the Teton Landscape, a Geological Chronicle of Jackson Hole and the Teton Range. Grand Teton Natural History Association, Moose, Wyoming. 132 pp., Revised 2007.

Machette, M.N., Pierce, K.L., McCalpin, J.P., Haller, K.M., Dart, R.L., 2001. Map and data for Quaternary faults and folds in Wyoming: U.S. Geological Survey Open File Report 01-461, map and 155 pages.

Miller, D.S., Smith, R.B., 1999. P and S velocity structure of the Yellowstone volcanic field from local earthquake and controlled-source tomography. J. Geophys. Res. 104, 15105–15121.

Morgan, L.A., McIntosh, W.C., 2005. Timing and development of the Heise volcanic field Snake River Plain, Idaho western USA. Geological Society of America Bulletin 117, 288–301.

Petersen, M.D., Frankel, A.D., Harmsen, S.C., Mueller, C.S., Haller, K.M., Wheeler, R.L., Wesson, R.L., Zeng, Y., Boyd, O.S., Perkins, D.M., Luco, N., Field, E.H., Wills, C.J., Rukstales, K.S., 2008. Documentation for the 2008 update of the United States National Seismic Hazard Maps: U.S. Geological Survey Open-File Report 2008-1128, 61 p.

Petrick, F. E., 2008. Scarp analysis of the Centennial normal fault, Beaverhead County, Montana and Fremont County, Idaho: M.S. thesis, Montana State University, Bozeman, Mt., 267 p.

Pierce, K.L., Morgan, L.A., 1992. The track of the Yellowstone hot spot—volcanism, faulting and uplift. In: Link, P.K., Kuntz, M.A., and Platt, L.W. (Eds.), Regional geology of eastern Idaho and western Wyoming: Geological Society of America Memoir 179, p. 1–53, 24 figs., 1 color map.

Pierce, K.L., Despain, D.G., Whitlock, C., Cannon, K.P., Meyer, G., Morgan, L., Licciardi, J.M., 2003. Quaternary geology and ecology of the Greater Yellowstone area. In: Easterbrook, D.J. (Ed.), Quaternary Geology of the United States, INQUA 2003 Field Guide Volume, pp. 313–344.

Pierce, K.L., Cannon, K.P., Meyer, G.A., Trebesch, M.J., Watts, Raymond, 2007. Post-glacial inflation-deflation cycles, tilting, and faulting in the Yellowstone caldera based on Yellowstone Lake shorelines. In: Morgan, L.A. (Ed.), Recent Contributions to the Geology of Yellowstone, U.S. Geological Survey Professional Paper 1717, Chapter E. 30 pp.

Puskas, C.M., Smith, R.B., Meertens, C.M., Chang, W.L., 2007. Crustal deformation of the Yellowstone–Snake River Plain volcanic system: campaign and continuous GPS observations, 1987–2004. J. Geophys. Res. 112, B03401. doi:10.1029/2006JB004325.

Reasenberg, P., 1985. Second-order moment of central California seismicity, 1969–1982. J. Geophys. Res. 90, 5479–5495.

Ruleman, C.A., 2002. Quaternary tectonic activity within the northern arm of the Yellowstone tectonic parabola and associated seismic hazards, southwest Montana: M.S. thesis, Montana State University, Bozeman, MT., 157 p.

Shuey, R.T., Ugland, R.O., Schmidt, C.R., 1977. Magnetic properties and secular variation in cores from Yellowstone and Jackson Lakes, Wyoming. J. Geophys. Res. 82, 3739–3746.

Smith, R.B., 1988. Seismicity and earthquake hazards of the Borah Peak–Hebgen Lake–Yellowstone–Teton region — implications for earthquakes in extensional and active volcanic regimes. Abstracts with Programs, Ann. Meeting, Geol. Soc. Amer, p. A12.

Smith, R.B., Sbar, M.L., 1974. Contemporary tectonics and seismicity of the western United States with emphasis on the Intermountain Seismic Belt. Bull. Geol. Soc. Am. 85 (8), 1205–1218.

Smith, R.B., Arabasz, W.J., 1991. Seismicity of the intermountain seismic belt. In: Slemmons, D.B., Engdahl, E.R., Zoback, M.D., Blackwell, D.D. (Eds.), Decade Map vol. 1 Neotectonics of North America. Geological Society of America, Boulder, Colo, pp. 185–228.

Smith, R.B., Braile, L.W., 1993. Topographic signature, space–time evolution, and physical properties of the Yellowstone–Snake River Plain volcanic system: the Yellowstone hotspot. In: Snoke, A.W., Steidtmann, J., Roberts, S.M. (Eds.), Geology of Wyoming: Geological Survey of Wyoming Memoir No. 5, pp. 694–754.

Smith, R.B., Richins, W.D., Doser, D.I, 1985. The Borah Peak earthquake: seismicity, faulting kinematics and tectonic mechanism. Workshop XXVIII on "The Borah Peak Earthquake," U. S. Geological Survey Open-File Report, vol. 85-290, pp. 236–263.

Smith, R.B., Byrd, J.O.D., Susong, D.D., Sylvester, A.G., Bruhn, R.L., Geissman, J., 1990. An evaluation of earthquake hazards of the Grand Teton National Park emphasizing the Teton fault. Three Year Progress Report, prepared for the University of Wyoming-National Park Service Research Center. University of Wyoming, Laramie, Wyoming. 149 pp.

Smith, R.B., Byrd, J.O.D., Susong, D.D., 1993. The Teton fault: seismotectonics, Quaternary history and earthquake hazards. In: Snoke, A.W., Steidtmann, J., Roberts, S.M. (Eds.), "Geology of Wyoming", Geological Survey of Wyoming Memoir No. 5, pp. 628–667.

Smith, R.P., Jackson, S.M., Hackett, W.R., 1996. Paleoseismology and seismic hazards evaluations in extensional volcanic terrains. J. Geophys. Res. 101 (B3), 6277–6292.
Smith, R.B., Jordan, M., Steinberger, R., Puskas, C., Farrell, J., Waite, G., Husen, S., Chang, W., O'Connell, R., Klingele, E., 2009. Geodynamics of the Yellowstone hotspot and mantle plume: seismic and GPS imaging, kinematics, and mantle flow. J. Volcanol. Geotherm. Res. 188, 26–56.
Spudich, P., Joyner, W.B., Lindh, A.G., Boore, D.M., Margaris, B.M., Fletcher, J.B., 1999. SEA99—a revised ground motion prediction relation for use in extensional tectonic regimes. Bull. Seismol. Soc. Am. 89, 1156–1170.
Thurber, C.H., 1983. Earthquake locations and three-dimensional crustal structure in the Coyote Lake area, central California. J. Geophys. Res. 88, 8226–8236.
U.S. Geological Survey and Idaho Geological Survey Resources, 2006. Quaternary fault and fold database for the United States. accessed Jan 23, 2006, from USGS web site: http//earthquake.usgs.gov/regional/qfaults/.
U.S. Geological Survey and Montana Bureau of Mines and Mineral Resources, 2006. Quaternary fault and fold database for the United States. Accessed Jan 23, 2006, from USGS web site:http//earthquake.usgs.gov/regional/qfaults/.
U.S. Geological Survey and Wyoming State Geological Survey Resources, 2006. Quaternary fault and fold database for the United States. accessed Jan 23, 2006, from USGS web site: http//earthquake.usgs.gov/regional/qfaults/.
Waite, G. P., 1999. Seismicity of the Yellowstone Plateau: space–time patterns and stresses from focal mechanism inversion. M.S. Thesis, University of Utah, Salt Lake City, UT.
Waite, G.P., Smith, R.B., 2002. Seismic evidence for fluid migration accompanying subsidence of the Yellowstone caldera. J. Geophys. Res. 107. doi:10.1029/2001JB000586.
Waite, G.P., Smith, R.B., 2004. Seismotectonics and stress field of the Yellowstone volcanic plateau from earthquake first-motions and other indicators. J. Geophys. Res. 109, B02301. doi:10.1029/2003JB002675.
Wald, D. J., Wald, L., Worden, B., Goltz, J., 2003. ShakeMap—A Tool for Earthquake Response, U.S. Geological Survey Fact Sheet 087-03.
Wells, D.L., Coppersmith, K.J., 1994. New empirical relationships among magnitudes, rupture length, rupture width, rupture area and surface displacement. Bull. Seismol. Soc. Am. 84, 974–1002.
White, B. J. P., 2006. Seismicity, Seismotectonics, and Preliminary Earthquake Hazard Analysis of the Teton Region, Wyoming. M.S. Thesis, University of Utah, Salt Lake City, UT.
Wiemer, S., Zuniga, R.F., 1994. ZMAP— a software package to analyze seismicity. Eos Trans. AGU 75, 456.
Wong, I.G., Olig, S.S., Dober, M., 2000. Preliminary probabilistic seismic hazard analyses: Island Park, Grassy Lake, Jackson Lake, Palisades, and Ririe Dams. U.S Department of the Interior, Bureau of Reclamation, Denver, Colorado.

Seismic Hazard Curves for Peak Ground Acceleration (g) for the Teton Area using Fault Slip Data Provided by JVGR Reviewer Kenneth L. Pierce

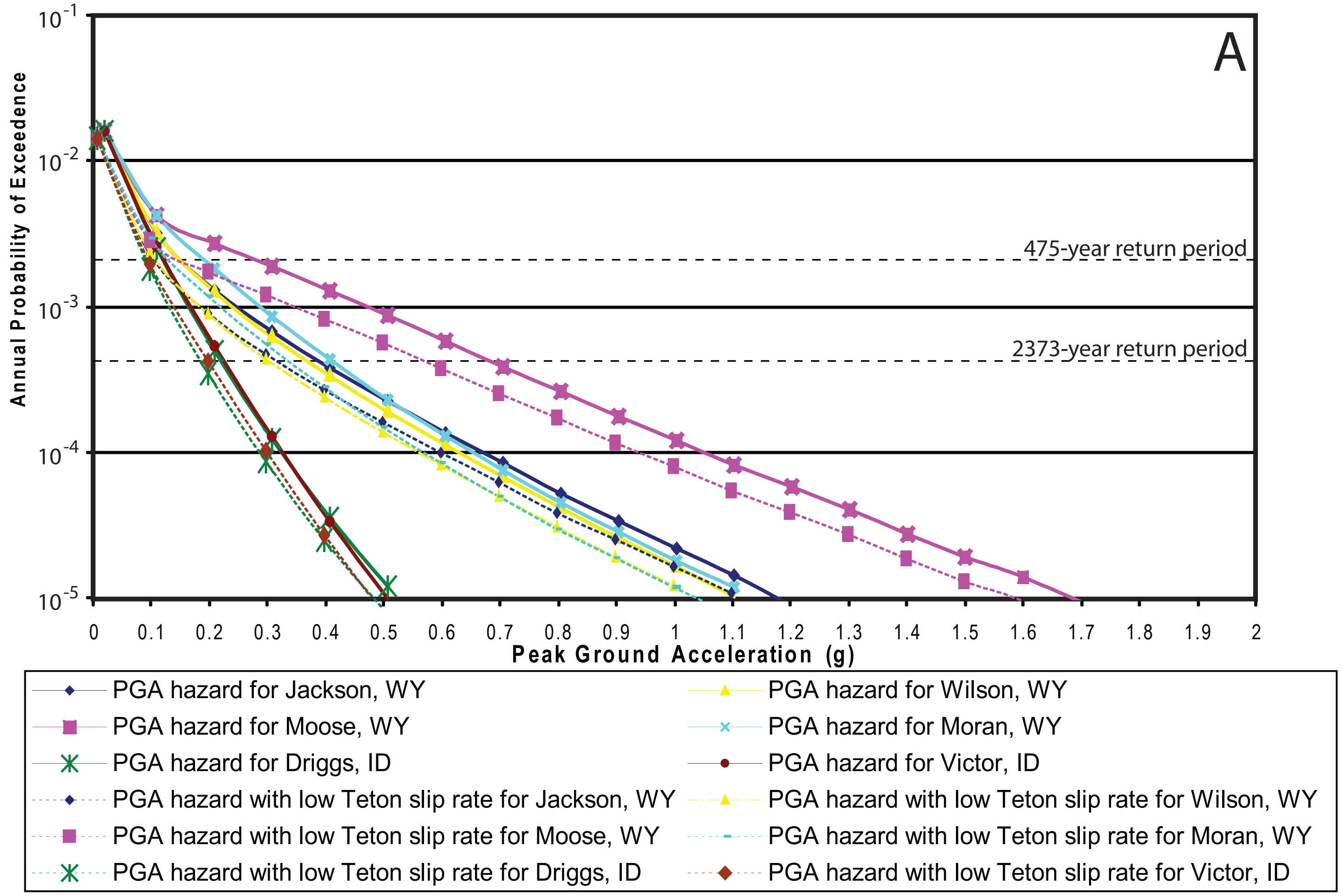

Seismic Hazard Curves for Peak Ground Acceleration (g) for the Yellowstone Area using Fault Slip Data Provided by JVGR Reviewer Kenneth L. Pierce

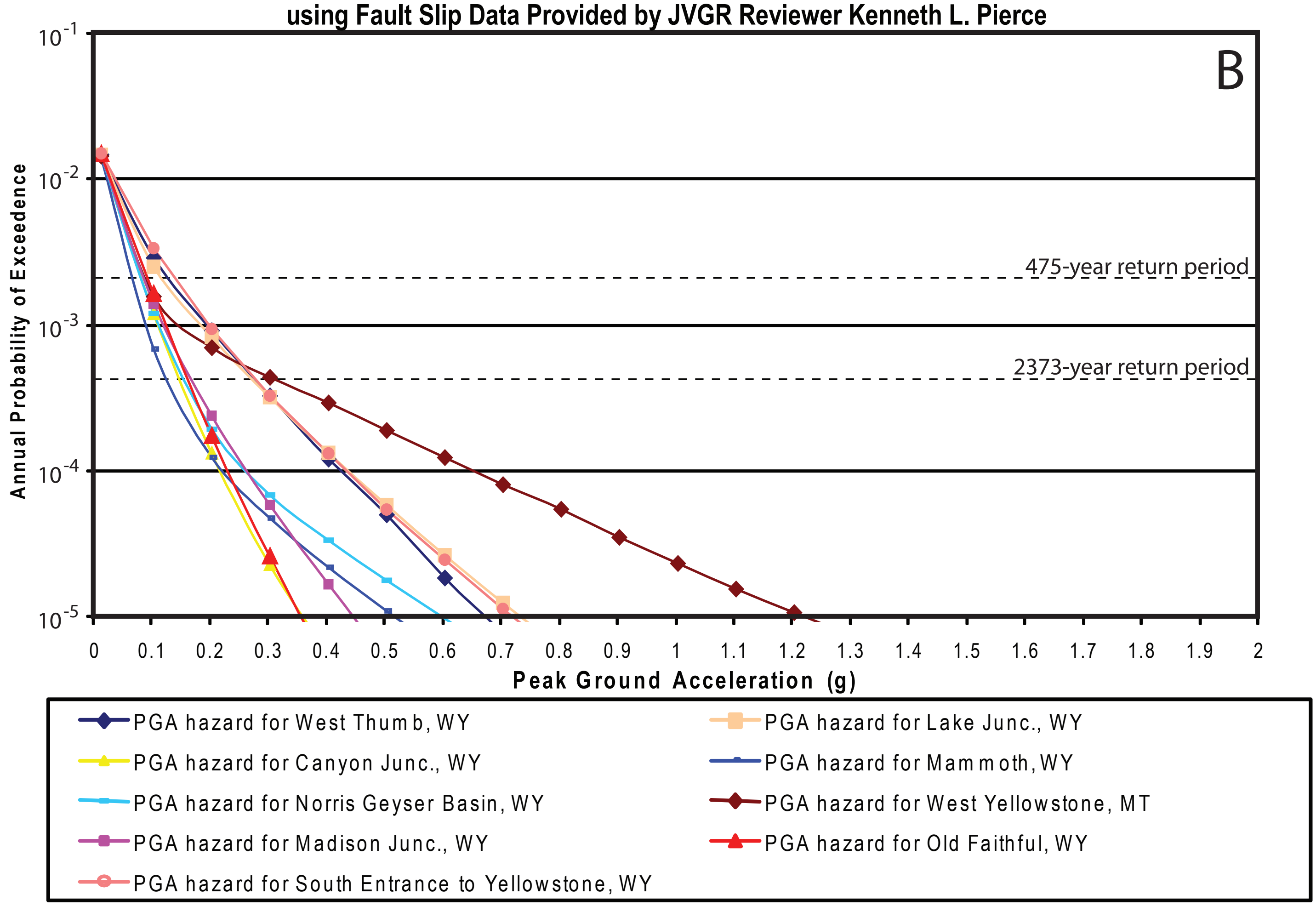

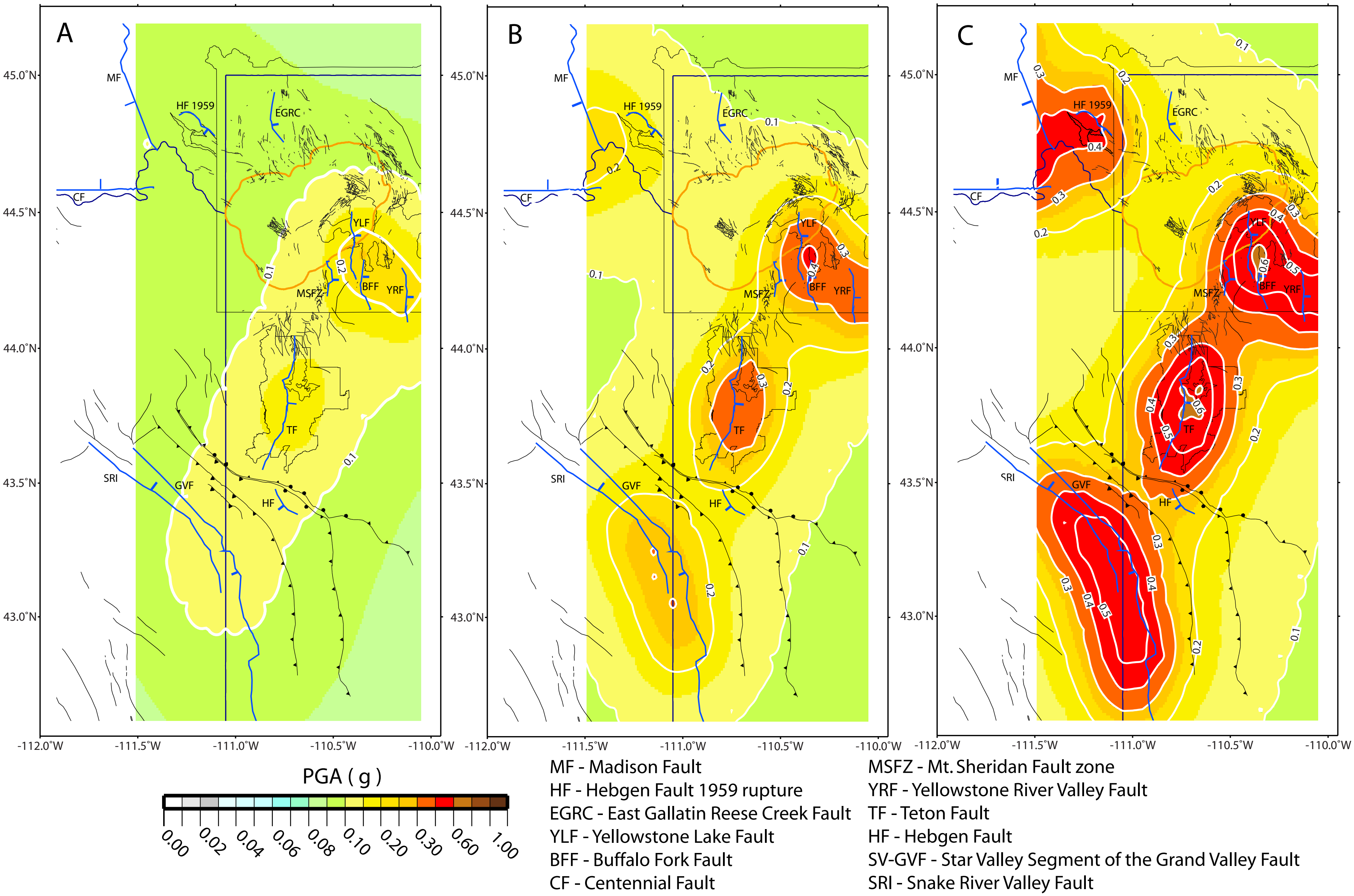

A
B
C
45.0°N
44.5°N
44.0°N
43.5°N
43.0°N
-112.0°W
-111.5°W
-111.0°W
-110.5°W
-110.0°W
MF
HF 1959
EGRC
CF
YLF
MSFZ
BFF
YRF
TF
SRI
GVF
HF
PGA (g)
0.00
0.02
0.04
0.06
0.08
0.10
0.20
0.30
0.60
1.00
MF - Madison Fault
HF - Hebgen Fault 1959 rupture
EGRC - East Gallatin Reese Creek Fault
YLF - Yellowstone Lake Fault
BFF - Buffalo Fork Fault
CF - Centennial Fault
MSFZ - Mt. Sheridan Fault zone
YRF - Yellowstone River Valley Fault
TF - Teton Fault
HF - Hebgen Fault
SV-GVF - Star Valley Segment of the Grand Valley Fault
SRI - Snake River Valley Fault

Supplemental Table 1 - Fault Slip Rates as Provided by Reviewer Kenneth L. Pierce

Fault Name	Faulting Type	Average Slip-Rate
Teton Fault	normal	1.36 mm/yr
Hoback Fault	normal	0.071 mm/yr
Star Valley Segment of the Grand Valley Fault	normal	0.82 mm/yr
Snake River Valley Fault	normal	0.002 mm/yr
Mount Sheridan Fault	normal	1.4 mm/yr
Buffalo Fork Fault	normal	0.2 mm/yr
Upper Yellowstone Valley Fault	normal	0.37 mm/yr
Yellowstone Lake Fault	normal	0.27 mm/yr
Centennial Fault	normal	0.6 mm/yr
Hebgen Fault	normal	0.5 mm/yr
Madison Fault	normal	1.0 mm/yr
East Gallatin Fault	normal	0.01 mm/yr